Loadings, chemical patterns and risks of inhalable road dust particles in an Atlantic city in the north of Portugal

Célia A. Alves[1*], Estela D. Vicente[1], Ana M.P. Vicente[1], Ismael Casotti Rienda[1], Mário Tomé[2], Xavier Querol[3], Fulvio Amato[3]

[1]Department of Environment, Centre for Environmental and Marine Studies (CESAM), University of Aveiro, 3810-193 Aveiro, Portugal

[2]PROMETHEUS, School of Technology and Management (ESTG), Polytechnic Institute of Viana do Castelo, Avenida do Atlântico nº 644, 4900-348 Viana do Castelo, Portugal

[3]Institute of Environmental Assessment and Water Research, Spanish Research Council, 08034 Barcelona, Spain

Abstract

Road dust resuspension has a significant contribution to the atmospheric particulate matter levels in urban areas, but loadings, emission factors, and chemical source profiles vary geographically, hampering the accuracy of emission inventories and source contribution estimates. Given the dearth of studies on the variability of road dust, in the present study, an in-situ resuspension chamber was used to collect PM_{10} samples from seven representative streets in Viana do Castelo, the northernmost coastal city in Portugal. PM_{10} samples were analysed for organic and elemental carbon by a thermo-optical technique, elemental composition by ICP-MS and ICP-AES, and organic constituents by GC-MS. Emission factors were estimated to be, on average, 340 and 41.2 mg veh^{-1} km^{-1} for cobbled and asphalt pavements, respectively. Organic carbon accounted for 5.56±1.24% of the PM_{10} mass. Very low concentrations of PAHs and their alkylated congeners were detected, denoting a slight predominance of petrogenic compounds. Si, Al, Fe, Ca and K were the most abundant elements. The calculation of various geochemical indices (enrichment factor, geoaccumulation index, pollution index and potential ecological risk) showed that road dust was extremely enriched and contaminated by elements from tyre and brake wear (e.g. Sb, Sn, Cu, Bi and Zn), while lithophile elements showed no enrichment. For As, the geochemical and pollution indices reached their maximum in the street most influenced by agricultural activities. Sb, Cd, Cu and As can pose a very high ecological risk. Sb can be regarded as the pollutant of highest concern, since it represented 57% of the total ecological risk. Hazard indices higher than 1 for some anthropogenic elements indicate that non-carcinogenic effects may occur. Except for a street with more severe braking, the total carcinogenic risks can be considered insignificant.

Keywords: road dust, resuspension, PM_{10}, metals, geochemical indices, health risk

* Corresponding author. E-mail: celia.alves@ua.pt

Introduction

According to data compiled by the World Health Organisation on particulate matter of diameter less than 10 (PM_{10}) and 2.5 µm ($PM_{2.5}$) for about 3000 cities and towns worldwide (WHO, 2016), globally, only 16% of the assessed population is exposed to PM_{10} or $PM_{2.5}$ annual mean levels complying with air quality guidelines (AQG). This increases to 27% for the interim target 3 (i.e. IT-3: 30 µg m^{-3} for PM_{10} and 15 µg m^{-3} for $PM_{2.5}$) of the AQG, 46% for interim target 2 (i.e. IT-2: 50 µg m^{-3} for PM_{10} and 25 µg m^{-3} for $PM_{2.5}$), and 56% for interim target 1 (IT-1: 70 µg m^{-3} for PM_{10} and 35 µg m^{-3} for $PM_{2.5}$). Based on more than 400 source apportionment records from studies conducted in cities of 51 countries, Karagulian et al. (2015) estimated the average contributions to ambient particulate matter. It was found that road traffic remains the biggest source of urban ambient air pollution, accounting for 25% of the global levels of this pollutant. Regulatory programmes aimed at reducing air pollution from road traffic have exclusively focused on tailpipe exhaust emissions. However, it has been shown that the contribution of non-exhaust primary particles to the total traffic generated airborne particulate material is significant in urban areas (Amato et al., 2014, 2016a; Font and Fuller, 2016; Guevara, 2016; Gulia et al., 2019; Harrison et al., 2012; Hooftman et al., 2016; Kalaiarasan et al., 2018; Padoan and Amato, 2018; Pant and Harrison, 2013; Yu et al., 2013). Non-exhaust emissions comprise tyre wear, brake wear, road surface wear and resuspension of road dust. A review by Denier van der Gon et al. (2013) found that the proportion between non-exhaust and exhaust particles strongly increased in the last two decades due to the successful implementation of exhaust emission control technologies and improvement of fuel quality. Aiming at quantifying exhaust/non-exhaust emissions, Lawrence et al. (2013) combined motorway tunnel sampling and source apportionment modelling. The application of principal component analysis and multiple linear regression analysis enabled to identify the emission sources for 82% of the total PM_{10} mass inside the tunnel. Among the identified sources, road dust resuspension was found to account for 27% of the PM_{10} mass. Weinbruch et al. (2014) quantified the contribution of the three traffic-related components (exhaust, abrasion, and resuspension) to curbside and urban background PM_{10} and PM_1 levels in the urban/industrial Ruhr area (Germany), based on the analysis of individual particles by scanning electron microscopy. The total contribution of traffic to PM_{10} was estimated to be 27% at the urban background station and 48% at the curbside station. Values for PM_1 were 15% and 39%, respectively. The relative share of the various traffic emissions for PM_{10} at the curbside station was 27% exhaust, 15% abrasion, and 58% resuspension (38%, 8%, 54% for PM_1). The relative shares for PM_{10} at the urban background were as follows: 22% exhaust, 22% abrasion and 56% resuspension (40%, 27%, 33% for PM_1). In comparison with previous studies described in the literature, Weinbruch et al. (2014) observed a significantly lower proportion of exhaust particles and a significantly higher proportion of resuspension particles. The high abundance of resuspension particles

emphasises their importance to the observed detrimental health effects of traffic emissions and the need to devise specific mitigation measures.

A stochastic model based on empirical probability distribution functions has been applied by Jazcilevich et al. (2012) to estimate human exposure to emissions from the resuspension of road dust due to isolated wakes from moving vehicles. Results showed that children are at higher risk than adults due to their lower height and higher respiratory intake rates during periods of light and moderate activity. Khan and Strand (2018) carried out a systematic literature review of articles on road dust and its effects on health. Several components of road dust particles were found to be associated with multiple health effects, especially on the respiratory and cardiovascular systems. Chronic obstructive pulmonary disease, asthma, fungal infections, allergies, carcinoma, and cardiovascular-related hospital admissions have been listed among the health outcomes.

Since exposure to particulate matter has been linked to adverse health effects by numerous studies, official entities have been intensely incentivising the market to switch to electric passenger cars, especially in Europe. However, a literature review by Timmers and Achten (2016) concluded that electric vehicles may not decrease levels of PM as much as expected, because of their relatively high weight. Several studies have shown a positive correlation between weight and non-exhaust emissions, although further research is required into the exact impact additional weight has on emission factors. Based on the available data, Timmers and Achten (2016) found that, when accounting for the additional weight and non-exhaust PM factors, total PM_{10} emissions from electric vehicles are equal to those of modern internal combustion engine vehicles, whilst for $PM_{2.5}$ emissions, plug-in cars deliver only a negligible reduction in emissions. Nevertheless, these differences are likely to vanish totally as exhaust emission standards become even stricter.

Together with dust from other sources, part of the non-exhaust particles settles and accumulate on road surfaces to form road dust, which is then resuspended by several inducers, such as wind and the wake of vehicles. Resuspended dust episodes are a common problem in many Nordic cities every spring, when the snow and ice have melted, and the streets have dried to expose the sand that has been spread during the winter to avoid slipperiness. Studded tyres, which are commonly used on vehicles in Scandinavian countries, erode the road surface and grind the sand particles. A similar effect is also observed for soil-derived particles in late autumn, possibly because of the change to studded tyres before the following winter months (Gustafsson et al., 2019; Hosiokangas et al., 2004). On the other hand, in Mediterranean countries and in other regions, where long periods without precipitation can be recorded, the dry weather conditions favour the resuspension of road dust (Amato et al., 2011, 2014; Pant et al., 2015). In addition, dust loadings and the chemical source profile vary geographically, depending on other parameters besides meteorology, such as traffic (volume and pattern, fleet characteristics), pavement type, and geology of the region (Amato et al., 2014; Gulia et al., 2019). Thus, to correctly apportion the contribution of road dust to ambient particulate matter, chemical profiles for each region should be used. Region-specific emission factors are also a condition for improving the accuracy of

emission inventories. There is a clear lack of data in the field of dust resuspension to conclusively assess its importance for air quality and the impact on human health. In Portugal, the scarce information available concerns samples obtained in 5 streets of Oporto (Alves et al., 2018). With the aim of broadening the representativeness of the available information, a new sampling campaign was carried out in another Portuguese city to determine road dust loadings and the chemical properties. This paper presents and discusses estimates of emission factors and the detailed elemental and organic composition of the thoracic fraction (PM_{10}) of road dust obtained from in situ measurements on pavements with different characteristics. Additionally, contamination indices and risks are assessed.

Methodology

Sampling

Road dust sampling took place in September and October 2018 on representative streets of Viana do Castelo (Fig. 1), the most northern Atlantic city in Portugal. The prevailing winds in this period are from the north, although in the end of October, the southern direction starts to dominate the records. To cause less disruption to traffic, sampling took place on Saturdays and Sundays, from 9:00 to 17:00, local time. With a population of about 90,000 inhabitants, Viana do Castelo lies between the estuary of the River Lima, the sea and the Santa Luzia hill. The city has a seaport with naval repairing and construction facilities and is home to a large cluster of wind green electricity and car-parts industries. These activities can represent sources of pollution, mainly of metallic constituents. Road traffic and some family farming in the vicinity of the city are other possible sources of pollution. Road dust samples were collected on the right lane of the street excluding the gutter where mass is not directly resuspended. To supervise traffic and ensure safety, all the sampling activities were conducted with the support of the police authorities. Sampling was carried out after a period of at least one week without rain. Unlike sweeping, street washing is not a routine practice in the city. However, to evaluate the effectiveness of water flushing in combination with sweeping on dust loadings, in one of the streets (Rua Alto Xisto, #1, with cobbled pavement), sampling was done before and repeated 24 hours after the cleaning operation.

Fig. 1. Map of the city of Viana do Castelo showing the location of the road dust sampling sites:
1 - Rua Alto Xisto - residential area on the outskirts of the city; cobbled pavement made of granite cubes
2 - Av. Capitão Gaspar de Castro - access road to the city centre and residential areas with various public facilities; stone mastic asphalt pavement
3 - Largo João Tomás da Costa - access to the city centre by the river front; stone mastic asphalt pavement
4 - Av. Combatentes da Grande Guerra - central artery connecting to the train station; cobbled pavement made of granite cubes
5 - Av. 25 de Abril - steep exit of a main thoroughfare that crosses the city to a residential neighbourhood; stone mastic asphalt pavement
6 - Av. do Atlântico - avenue of access to the main beach of the city, next to the shipyards; stone mastic asphalt pavement
7 - ESTG - local road within the campus of the Higher School of Technology and Management; stone mastic asphalt pavement

The thoracic fraction of road dust was directly vacuumed in situ, at an air flow rate of 25 L min^{-1}, using a rotary vane pump (VTE Series Picolino, Gardner Denver Thomas, Germany), which was connected to a field resuspension chamber (Amato et al., 2009a, 2011). With this apparatus, road dust is resuspended in a methacrylate deposition chamber, while particles small and/or light enough to be carried by the air stream continue their path through the system, entering a Negretti stainless steel elutriation filter that was designed to allow the passage of only PM_{10}. These are finally collected on a 47 mm diameter filter (quartz fibre, Pallflex®), while particles with aerodynamic diameter > 10 μm are deposited in the methacrylate chamber and along the elutriation filter. Sampling was performed in surface areas of 1 m^2 for 30 min. Aiming at minimising casual errors and obtaining enough material for the subsequent chemical analyses, in each street, at least three independent replicate samples were collected onto different filters. Before the gravimetric quantification, filters were calcined at 500 °C for 6 h and conditioned for around 24 h in a room with controlled humidity (50%) and temperature (20 ºC).

163 The weightings were performed with an analytical balance (RADWAG 5/2Y/F, Poland) and obtained
164 from the average of six measurements (relative standard deviation < 0.02%).
165
166 ***Chemical analyses***
167
168 Two punches of 9 mm were used to quantify the organic (OC) and elemental carbon (EC) content
169 of each filter by a thermal optical transmission technique. The filter punches were first subjected to a
170 controlled heating in a non-oxidising nitrogen atmosphere to volatilise the OC. The second step
171 consisted of the EC oxidation in a nitrogen and oxygen atmosphere. The measurement of the light
172 transmittance through the filter allows separating the EC formed by pyrolysis of the OC during the first
173 step from the one that was originally present in the sample. The CO_2 released from the thermal
174 volatilisation and oxidation of different carbon fractions was quantified by a non-dispersive infrared
175 analyser.
176 Two 9 mm punches of each filter were used to analyse trace and major elements. The punches of the
177 different replicate samples of each street were combined and digested together. The digestion was
178 performed in closed Teflon 60 mL reactors by using a 1.25 mL HNO_3: 2.5 mL HF: 1.25 mL $HClO_4$
179 mixture. Then, samples were subjected to evaporation, and final re-dissolution with HNO_3, after which
180 they were analysed for a total of around 60 elements. The international reference material NBS1633b
181 was also digested to determine the accuracy of the analytical and digestion methods. Levels of trace
182 elements in completely dissolved samples were determined by inductively coupled plasma atomic
183 emission spectroscopy (ICP-AES, Thermo Scientific, iCAP 6500 Radial) and/or inductively coupled
184 plasma mass spectroscopy (ICP-MS, Thermo Scientific, X-Series II). To create external calibration
185 curves, three multi-elemental solutions (Spec® 1 - rare earth elements, Spec® 2 - alkalis, earth alkalis,
186 and metals, and Spec® 4 - Nb) were used. To control the mean precision and accuracy, repeated
187 analyses of 0.025 mg of NBS1633b (fly ash) reference material (NIST, Gaithersburg, MD, USA) were
188 carried out. They fell in the ranges 3–5% and <10% for ICP-AES and ICP-MS, respectively. For most
189 trace elements, the detection limits were 0.01 ng m^{-3}.
190 For each road, the remaining portions of the filters were combined and extracted three times with
191 dichloromethane in an ultrasonic bath (25 mL for 15 min, each extraction, with 5 min stops between
192 them). After each extraction, the organic extracts of each composite sample were combined, filtered
193 through pre-cleaned cotton and concentrated to a volume of 0.5 mL using a Turbo Vap® II evaporation
194 system (Biotage, Charlotte, NC, USA). The concentrated samples were transferred into vials and dried
195 under a gentle nitrogen stream. Polycyclic aromatic compounds (PAHs) and phthalates (plasticisers)
196 were determined in a gas chromatographer-mass spectrometer from Agilent (GC model 7890B, MS
197 model 5977A) with single quadrupole, a CombiPAL autosampler and a Tekno TRB-5MS (60 m × 0.25
198 mm × 0.25 μm) column. Data were acquired in the electron impact (EI) mode (70 eV) using helium as
199 carrier gas at 1 mL min^{-1}. The oven temperature programme was as follows: 60 °C (1 min), 60–150 °C

(10 °C min^{-1}), 150–290 °C (5 °C min^{-1}), 290 °C (30 min). The quantitative analysis was performed by single ion monitoring (SIM). For the determination of PAHs, a mixture of deuterated internal standards (IS) was used: 1,4-dichlorobenzene-d4, naphtalene-d8, acenaphthene-d10, phenanthrene-d10, chrysene-d12, perylene-d12, fluorene-d10 and benzo[a]pyrene-d12 (Supelco). The IS used in the case of plasticisers were the deuterated diethyl phthalate-3,4,5,6-d4 and bis(2-ethylhexyl)phthalate-3,4,5,6-d4 (Supelco). Calibration was based on a total of 30 authentic standards (Sigma-Aldrich) in five different concentration levels. Additional details on standards and their quantification ions used in the SIM mode are given in Tables S1 to S4.

Estimation of emission factors

To roughly estimate PM_{10} emissions from road dust resuspension, the empirical relationship derived by Amato et al. (2011) was employed:

$$EF = 45.9 \times RD^{0.81} \quad (1)$$

where,

EF = PM_{10} emission factor (milligrams per vehicle and kilometre travelled, mg veh^{-1} km^{-1}),

RD = PM_{10} road dust loadings (mg m^{-2}).

Geochemical indices

Enrichment factors have been extensively used to determine the degree of enrichment due to anthropogenic activities in road dust, and separate possible natural from human sources. Enrichment factors of each element with respect to crustal material (Wedepohl, 1995) were calculated using Al as reference element:

$$\text{Enrichment Factor} = (X/Al)_{air}/(X/Al)_{crust} \quad (2)$$

where $(X/Al)_{air}$ is the concentration ratio of the element X to Al in the PM_{10} samples, and $(X/Al)_{crust}$ is the average concentration ratio of X to Al in the continental crust. In general, based on the enrichment factors, five contamination categories are considered: < 2 minimal enrichment, [2,5[moderate enrichment, [5,20[significant enrichment, [20,40[very high enrichment, and ≥ 40 extremely high enrichment (Yang et al., 2016).

The contamination levels of heavy metals in road dust can also be evaluated by the geoaccumulation index (I_{geo}):

$$I_{geo} = \log_2 \frac{C_n}{1.5B_n} \quad (3)$$

where C_n represent the concentration of an element in the dust, and B_n is the geochemical background value of the same element. In this study, the mean concentration of elements in the upper continental crust was used as B_n (Wedepohl, 1995), since standard background values for Portuguese soils or dusts are not available. Based on the I_{geo} values, the contamination levels are classified into seven classes (Cai and Li, 2019; Zgłobicki et al., 2019): class 0, uncontaminated ($I_{geo} < 0$); class 1, uncontaminated to moderately contaminated ($0 \leq I_{geo} < 1$); class 2, moderately contaminated ($1 \leq I_{geo} < 2$); class 3, moderately to heavily contaminated ($2 \leq I_{geo} < 3$); class 4, heavily contaminated ($3 \leq I_{geo} < 4$); class 5, heavily to extremely contaminated ($4 \leq I_{geo} < 5$); and class 6, extremely contaminated ($I_{geo} \geq 5$).

Like enrichment factors and I_{geo}, the pollution index (PI) is also employed in numerous studies to assess the level of contamination of metals in soil or dust. It is given by the following ratio:

$$PI = \frac{C_n}{B_n} \quad (4)$$

The pollution index is classified into five groups (Wu et al., 2014): low ($PI < 1$), moderate ($1 \leq PI < 3$), considerable ($3 \leq PI < 6$), very high ($6 \leq PI < 12$) and extremely high ($PI \geq 12$). In addition, to give an assessment of the overall pollution status, the integrated pollution load index (PLI) can be employed, where n is the number of elements analysed (Chen et al., 2015):

$$PLI = (PI_1 \times PI_2 \times PI_3 \times \ldots \times PI_n)^{1/n} \quad (5)$$

The integrated pollution load index is divided into seven levels from none to high pollution to specify the contamination degree: background concentration ($PLI = 0$), unpolluted ($0 < PLI \leq 1$), unpolluted to moderately polluted ($1 < PLI \leq 2$), moderately polluted ($2 < PLI \leq 3$), moderately to highly polluted ($3 < PLI \leq 4$), highly polluted ($4 < PLI \leq 5$), or very highly polluted ($PLI > 5$).

The potentially harmful effects of heavy metals can be evaluated by calculating the potential ecological risk factor of individual metals (E_{ri}) and of multiple metals ($RI = \Sigma E_{r_i}$). The ecological risk factor is defined as follows:

$$E_{r_i} = T_i \times PI \quad (6)$$

T_i is the toxic-response factor for the metal. The values available in the literature are (Chen et al., 2019; Wang et al., 2018; Zgłobicki et al., 2019): Cd, 30; As, 10; Sb, 7; Cu, 5; Ni, 5; Pb, 5; Co, 5; Cr, 2; V, 2; Zn, 1; Mn, 1; Ba, 1. Five categories of pollution are distinguished (Chen et al., 2019; Zgłobicki et al., 2019): low ($E_{ri} < 40$), moderate ($40 \leq E_{ri} < 80$), considerable ($80 \leq E_{ri} < 160$), high ($160 \leq E_{ri} < 320$) and very high ($E_{ri} \geq 320$). The potential ecological risk (RI) is defined as the sum of the index of ecological risk factors (E_{ri}) for specific metals in a sample. Four categories are recognised (Chen et al., 2019; Zgłobicki et al., 2019): low ($RI < 150$), moderate ($150 \leq RI < 300$), considerable ($300 \leq RI < 600$) and high ($RI > 600$).

Human exposure risk assessment

Human exposure to metals and metalloids in road dust particles can occur via three main pathways: (a) hand to mouth ingestion, (b) dermal absorption, and (c) inhalation through the mouth and nose. Based on methodologies defined by the United States Environmental Protection Agency (USEPA), the average daily dose through ingestion (ADD_{ing}), inhalation (ADD_{inh}) and dermal contact (ADD_{dermal}) can be calculated as follows (Adimalla, 2020; and references therein):

$$CDD_{ing} = \frac{C \times IR_{ing} \times ED \times EF}{BW \times AT} \times CF \quad (7)$$

$$CDD_{inh} = \frac{C \times IR_{inh} \times ED \times EF}{BW \times AT \times PEF} \quad (8)$$

$$CDD_{derm} = \frac{C \times SA \times SAF \times DAF \times ED \times EF}{BW \times AT} \times CF \quad (9)$$

where C is the mass fraction of each element in road dust (mg kg^{-1}), IR_{ing} is the ingestion rate, IR_{inh} is the inhalation rate, ED is the exposure duration, EF is the exposure frequency, CF is a conversion factor, PEF is the particle emission factor, SA is the exposed skin surface area, SAF is the skin adherence factor, DAF is the dermal absorption factor, BW is the average body weight, and AT is the average time. Units and reference values for all these parameters are given in Table S5.

The hazard quotient (HQ) is typically used to assess the non-carcinogenic risk. It is calculated as the ratio of the chronic daily dose (CDD) and the reference dose (R_fD, mg kg^{-1} day^{-1}) for a given substance (Table S6). The total non-carcinogenic risk for the three exposure pathways for a single element is represented by the hazard index (HI), which is the sum of HQ_{ing}, HQ_{inh} and HQ_{derm}. HI values > 1 indicate a chance that non-carcinogenic effects may occur, whilst values < 1 express low or no risk of non-carcinogenic effects on humans.

The carcinogenic risk represents the possibility of an individual developing any type of cancer in the whole lifetime due to exposure to carcinogenic hazards. The carcinogenic health risk (CR) for a specific heavy metal is obtained as follows:

$$CR = CDD \times SF \quad (10)$$

where SF is the slope factor (mg kg^{-1} day^{-1}) for carcinogenic metals (As, Cd, Co, Cr and Ni). The total carcinogenic risk (TCR) is the sum of CR values for single metals. According to USEPA, values between 1×10^{-6} and 1×10^{-4} are taken as acceptable or tolerable cancer risks, while values lower than 1×10^{-6} indicate no significant health hazard. If TCR > 1×10^{-4}, the risk is unacceptable. The reference values of carcinogenic risk through dermal exposure and ingestion are not provided by the USEPA, so the cancer risks for these two exposure pathways cannot be estimated. The cancer slope factors for inhalation are listed in Table S6.

Results and Discussion

Road dust loadings and emission factors

According to what was previously observed in Paris (Amato et al., 2016b) and Oporto (Alves et al., 2018), granite cobblestone streets showed much higher RD loadings than asphalt pavements (Fig. 2). The higher roughness of cobblestones promotes the build-up of road sediments. In addition, the joints between granite cubes are filled with soil, which is prone to resuspension. Gustafsson et al. (2009) made measurements of PM_{10} in a road simulator to study the influence of three pavements with different aggregate sizes (granite < 16 mm, quartzite < 16 mm and quartzite < 11 mm). The granite pavement produced PM_{10} concentrations that were almost 70% higher in comparison to the quartzite pavement. The street paved with granite cobblestones in the city centre presented higher RD loading compared to the one located in a residential area on the outskirts. A higher number of vehicles in circulation and stop-and-go traffic at rush hours may have contributed to higher values on the downtown street. Among the asphalt roads, the one with the highest RD loadings (3.41±0.64 mg m^{-2}), value up to 6 times higher than on other streets with similar pavement, is an exit route from a main artery to a residential area. The slope of the track forces to decelerate, leading to higher brake and tyre wear. Mean RD values from 0.53 to 1.87, averaging 1.06 mg m^{-2}, were obtained for the remaining asphalt paved roads. Loadings of 0.48 ± 0.39 mg m^{-2} were reported for this type of pavements in Oporto (Alves et al., 2018). RD values of the same order as those observed in Portuguese cities were measured in Paris (0.66-2.43 mg m^{-2}, Amato et al., 2016b) and Zürich (0.2-1.3 mg m^{-2}, Amato et al., 2009a), while higher levels were recorded in the Spanish cities of Barcelona (3.7-23.1 mg m^{-2}) and Girona (1.3-7.1 mg m^{-2}) (Amato et al., 2009a). Average PM_{10} mass loading on the road surface was found to be much higher in New Delhi compared to Birmingham: 9.34±5.56 mg m^{-2}, 12.1±9.3 mg m^{-2} and 72.9±24.3 mg m^{-2} for sites A (UK roadside), B (UK road tunnel), and C (India roadside), respectively (Pant et al., 2015).

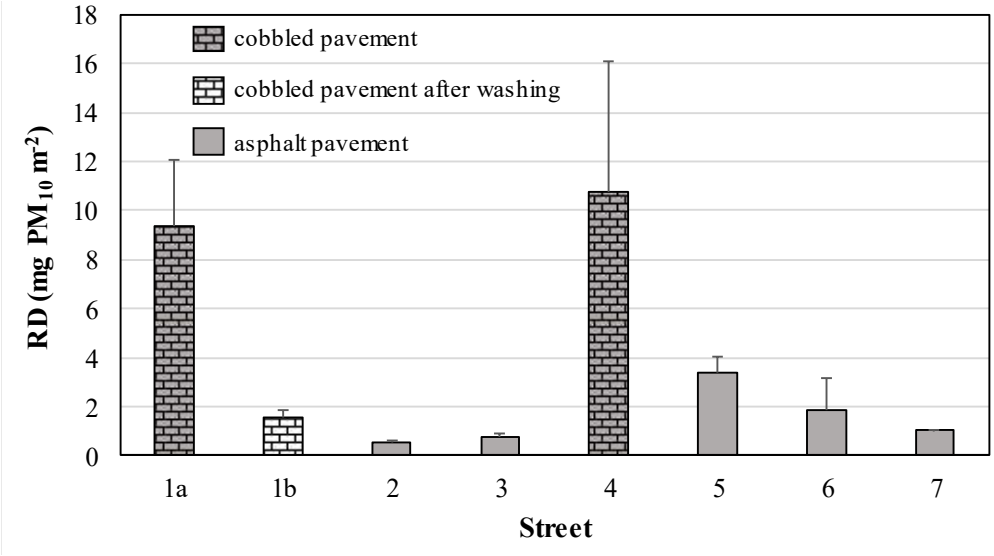

Fig. 2. Road dust loadings measured in the city of Viana do Castelo

High pressure washing in the early morning, in combination with sweeping, in one of the streets (Rua Alto Xisto, #1), contributed to a decrease of the RD loadings from 9.35±2.69 to 1.58±0.28 mg m^{-2}, representing a reduction efficiency of 83%. Street washing has been considered by several studies as able to reduce the mobility of dust load deposited on street surfaces and therefore being a potential effective measure for abating dust resuspension (Amato et al., 2009b, 2010; Chang et al., 2005; Chou et al., 2007; Karanasiou et al., 2011). When water adheres to deposited particles, it increases their mass and surface tension forces, reducing the likelihood of suspension and transport, especially as cohesion of wetted particles often persists after the water has evaporated due to the formation of aggregates (Watson et al., 2000).

Based on Eq. (1), emission factors for the PM_{10} fraction of road dust were estimated to be, on average, 340 and 41.2 mg veh^{-1} km^{-1} for cobbled and asphalt pavements, respectively. Values from 12.0 to 29.4 mg veh^{-1} km^{-1}, averaging 18.6 mg veh^{-1} km^{-1}, were derived for asphalt roads of Oporto, while an EF as high as 1082 mg veh^{-1} km^{-1} was obtained for a cobbled pavement in the same city (Alves et al., 2018). Typical urban roads in Milan were found to have fleet-averaged emission factors in the range 13-32 mg veh^{-1} km^{-1} (Amato et al., 2017). EFs of 14-23 mg veh^{-1} km^{-1} were documented for the UK mixed fleet (Thorpe et al., 2007). Values up to more than 200 mg veh^{-1} km^{-1} have been reported for Nordic conditions, although strong seasonal variations are observed due to studded tyres and the use of sand/salt as anti-skid treatment (Ketzel et al., 2007). It is noteworthy, however, that the available information is scarce and, in some cases, out of date, so additional measurements are required.

PM_{10} chemical composition

Organic carbon accounted for 5.56 ± 1.24 % of the PM_{10} mass (Table 1). A comparable mass fraction of 7.14 ± 3.48% was obtained in PM_{10} from resuspended road dust sampled in Oporto (Alves et al., 2018). Higher percentages (13-29%) were reported for the thoracic fraction of road dust in Bogota (Ramírez et al., 2019) and for three European cities (Amato et al., 2011): Girona (10.9 ± 5.2%), Barcelona (11.7 ± 1.8%) and Zurich (21.4 ± 12.5%). In Viana do Castelo, irrespective of the road, EC represented a minor mass fraction of PM_{10} (always < 0.40%). Small EC mass fractions were also obtained in Bogota (0.2-1.9%). In the previous sampling campaign in Oporto, percentages of 0.4% and 4.6 ± 0.8% were determined for a cobbled street and for asphalt paved roads, respectively. It should be borne in mind that, in the present study, the non-quantification of existing carbonate carbon may have slightly biased the thermal-optical OC and EC determination. On the other hand, the presence of certain minerals, such as Fe oxides, in samples may have complicated the laser correction for pyrolysis.

Elements, in the form of their most common oxides (SiO_2, Al_2O_3, MgO, MnO, Fe_2O_3, TiO_2, K_2O, etc.) accounted for 70% of the PM_{10} mass, on average. Since quartz filters are made of silica fibres, silicon has not been analysed. SiO_2 was estimated as $3\times Al_2O_3$ (Brines et al., 2016). Si, Al, Fe, Ca and K were the most abundant elements. Table S8 (Supplementary Material) provides information on the minimum and maximum values for the mass fractions of each element in road dust samples. Figure S2 depicts the spatial distributions of some elements.

Table 1. Mass fractions of carbonaceous constituents, major and trace elements in road dust < 10 μm (mean ± SD)

	%
OC	5.56 ± 1.24
EC	0.23 ± 0.12
SiO_2	38.9 ± 22.6
Al_2O_3	13.0 ± 7.52
Fe	5.15 ± 2.41
Ca	2.27 ± 2.00
K	1.90 ± 1.19
S	0.76 ± 0.86
Na	0.74 ± 0.39
Mg	0.52 ± 0.25
P	0.22 ± 0.09
Ti	0.63 ± 0.30
	μg g^{-1}
Li	232 ±106

Be	3.56 ± 4.58
Sc	18.3 ± 9.86
V	105 ± 52.0
Cr	296 ± 281
Mn	1029 ±437
Co	18.4 ± 9.70
Ni	110 ± 123
Cu	1816 ± 1138
Zn	2162 ± 1151
Ga	33.6 ± 17.7
Ge	7.86 ± 7.59
As	100 ± 48.0
Se	7.08 ± 9.69
Rb	386 ± 195
Sr	284 ± 125
Y	24.5 ± 10.2
Zr	232 ± 149
Nb	33.2 ± 14.4
Sn	314 ± 231
Sb	135 ± 134
Cs	35.5 ± 16.7
Ba	1845 ± 1263
La	59.0 ± 37.2
Ce	110 ± 70.5
Pr	11.9 ± 11.0
Nd	51.9 ± 31.9
Sm	19.1 ± 9.36
Gd	17.1 ± 9.98
Dy	6.31 ± 2.51
Er	1.57 ± 2.39
Hf	6.33 ± 3.73
Tl	0.757 ± 1.54
Pb	276 ± 164
W	28.0 ± 32.2

Bi	19.8 ± 13.9
Th	29.1 ± 18.7
U	26.4 ± 9.04

372

373 Given the low OC concentrations, many of the organic compounds analysed showed levels
374 equivalent to those detected in blanks (Table 2). PAH concentrations varied significantly from road to
375 road. In addition to different source strengths, the variation may be due to diverse meteorological and
376 atmospheric conditions. Degradation of PAHs accelerates with increasing temperature, sunlight and
377 levels of atmospheric oxidants. High molecular weights with ≥ 4 rings represented, on average, 48.3%
378 of total PAHs, whereas low molecular weights with 3 rings were more abundant (51.7%). This suggests
379 a slight predominance of petrogenic over pyrogenic sources (Casal et al., 2014). Mutagenic (MEQ) and
380 carcinogenic (TEQ) equivalents were calculated by multiplying the concentrations of each PAH with
381 its mutagenic and carcinogenic equivalency factors (MEF and TEF) relative to benzo(a)pyrene,
382 respectively. MEF and TEF values are provided in Table S7. On average, carcinogenic and mutagenic
383 equivalents accounted for 12.8 and 13.9% of the total PAH concentrations. Benzo[a]pyrene was the
384 compound that most contributed to the carcinogenic equivalent concentration, accounting for 91% of
385 the total, followed by dibenzo[a,h]anthracene with a contribution of only 1.5%. Mutagenic equivalents
386 were also dominated by benzo[a]pyrene (84%), while benzo[g,h,i]perylene had the second highest share
387 (10%).

388 Various alkylated PAHs were present in road dust, among which dimethylphenanthrenes were the
389 most abundant. The same semi-volatile alkyl PAHs have been detected in significant amounts in
390 particulate matter samples from the emissions of engines employing standard diesel, commercial diesel
391 and biodiesel B20 (Casal et al., 2014). Retene was also found in some road dust samples from Viana
392 do Castelo. Although, in the past, this alkylated phenanthrene has been identified as a good tracer of
393 coniferous combustion, it was recently associated with vehicle non-exhaust emissions (e.g. wear
394 particles from the interaction between tyres and pavements), with a probable origin in the natural waxes
395 and resins added as softeners and extenders to the rubbers (Alves et al., 2020). Benzothiazole, formerly
396 pointed out as a good tracer for tyre wear particles (Wik and Dave, 2009), was detected at mass fractions
397 ranging from 37.0 to 926 μg g^{-1} PM_{10}. This aromatic heterocyclic compound and its derivates are
398 commonly used as vulcanisation accelerators in rubber production and have been found in wear
399 particles from different tyre brands (Zhang et al., 2018). Nevertheless, the partitioning between the gas
400 and particulate phases is temperature dependent. Thus, the semi-volatility of these compounds raises
401 questions about their suitability as tracers of tyre wear. Carbazole was another aromatic heterocyclic
402 hydrocarbon present in PM_{10} from road dust. It has been identified as a product of tyre combustion
403 (Wang et al., 2007). Bis(2-ethylhexyl) phthalate stood out among plasticisers detected in the thoracic
404 fraction of street dust. Plasticisers, such as phthalates, are extensively applied in building materials,

405 personal care products, food packaging materials and textiles to improve the ductility and plasticity of
406 products. Some plasticisers (synthetic organic oils and resins) are used as components or additives to
407 provide elasticity and stickiness to the tyre and have been detected in both road particles and tread wear
408 particles (Vogelsang et al., 2019).
409
410 Table 2. Organic compounds quantified in road dust samples (values in μg g^{-1} PM_{10})

	min	max	avg
3 ring PAHs	nd	3.02	1.14
4 ring PAHs	nd	1.95	0.481
5 ring PAHs	nd	1.84	0.421
6 ring PAHs	nd	0.508	0.164
Methylnaphthalenes	nd	0.016	0.002
Dimethylnaphthalenes	nd	0.147	0.027
Methylfluorenes	0.061	6.33	0.597
Trimethylfluorenes	nd	0.042	0.009
Methylphenantrenes	0.006	2.16	0.524
Dimethylphenantrenes	0.299	11.9	2.76
Trimethylphenanthrenes	nd	16.2	2.50
Retene	nd	0.397	0.154
Carbazole	0.032	2.07	0.648
Benzothiazole	37.0	926	367
Di-n-butyl phthalate	nd	250	51.7
Benzyl butyl phthalate	0.248	20.2	7.37
Bis(2-ethylhexyl) adipate	nd	7.95	3.27
Bis(2-ethylhexyl) phthalate	286	1918	957
Di-n-octyl phthalate	nd	349	72.5
Diisononyl phthalate	nd	714	208

411 nd – not detected or of the same order of the blanks
412
413 ***Contamination indices and source ratios***
414
415 While minimal enrichments were always obtained for elements such as Mg, Na and K, very or
416 extremely high factors were registered for Cu, Zn, Sn, Sb, As, Se and Bi (Fig. S3). In the four most
417 central streets, Cd and Pb were also very highly enriched relative to naturally derived mineral dust.
418 Moreover, in the 3 streets closest to the shipyards, very or extremely high enrichment factors were
419 recorded for W. Emissions from this industrial activity may also have contributed to the sulphur
420 enrichment in road dust samples from the adjacent road.

Many of the anthropogenic elements with very high enrichment factors are emitted in tyre and brake wear processes. Despite the large variation in the chemical composition of commercial brake lining materials, most researchers have reported Fe, Cu, Zn and Pb as the most abundant metals (Grigoratos and Martini, 2015; and references therein). In the present study, Fe showed no enrichment in road dust from the two streets with less traffic intensity, suggesting a low anthropogenic influence and a significant geogenic contribution. Moderate enrichment factors in the busiest streets indicate that Fe particles from the abrasion of brake pads supplant the edaphic contribution. It has been found that brake linings and brake abrasion particles are also major sources of Sb. This element is used in the form of Sb_2S_3 as a lubricant to reduce vibrations and to improve friction stability. During the braking process, Sb_2S_3 is oxidised to Sb_2O_3, which has been described as a probable human carcinogen (von Uexküll et al., 2005). Other metal sulphides, such as SnS, Bi_2S_3, CuS, CuS_2 and PbS, are frequently applied in brake pad formulations to provide friction stability and to reduce wear at elevated temperatures (Österle and Dmitriev, 2016). Several trace elements (e.g. Cd, Cu, Pb, Zn), which are employed in tyre manufacture, have been identified in wear particles from this vehicle component (Penkała et al., 2018). Among these, Zn has been extensively used as a marker for tyre wear (Klöckner et al., 2019). Although manufacturers keep secrecy about the exact composition of the tyres, it is known that ZnO is the main vulcanisation agent. More than 50% of the ZnO global annual production (25 million tons annually) is used in rubber manufacturing with tyres representing its primary destination. Although in lesser quantities, a variety of organozinc compounds is also added to tyre tread rubber to facilitate vulcanisation (Mostoni et al., 2019). The enrichment of Se in many roads may result from atmospheric deposition of emissions from anthropogenic sources, which comprise combustion (coal, oil, wood, biomass, incineration, etc.), nonferrous metal melting, manufacturing and utilisation of agriculture products (Wen and Carignan, 2007). Bismuth was another element highly enriched in road dust. Among the countless uses, Bi is an ingredient in lubricating greases, a catalyst for making synthetic fibres and rubber, a constituent included in the formula for making dragon eggs firework stars, and a component of BSCCO (bismuth strontium calcium copper oxide), which is a high-temperature superconductor material applied in power cables, motors, generators, transformers, etc. (Sanderson, 2019).

Rare Earth elements (REE), such as La, Ce, Pr, Nd and Sm, showed very high correlations between them, with major elements of the Earth's crust (Al, K, Na and Mg), as well as with W, Th and P (Table S9). Phosphorus is found in the soil in organic compounds and in minerals. Thorium is a naturally occurring, slightly radioactive metal, found in small amounts in most rocks and soils. Tungsten is a rare metal found naturally on Earth combined with other elements. REE and major elements of the Earth's crust were also correlated with Ti, V and Cs. Despite being one of the most abundant elements in the Earth's crust, Ca correlated with Cu, Zn and Sn, suggesting an anthropogenic origin in brake and tyre wear. Sn, Sb, Fe, Cu, Ba, Zn, Bi, Er, Zr and Yb were strongly correlated between them pointing to these vehicle non-exhaust emissions as a common source.

Ratios between elements can be used to differentiate sources (Pant et al., 2015; Ramírez et al., 2019). Table 3 compares some ratios of the present study with those obtained for other regions. Cu/Sb ratios between 3.3 and 9.1 have been used to identify brake wear in PM collected in Cologne, London, Stockholm, Budapest and London (Dong et al., 2017; and references therein), while a ratio of 45 has been tabulated for the upper crust (Wedepohl, 1995). However, large discrepancies in this ratio due to variations in brake pad composition have been reported (Grigoratos and Martini, 2015). In fact, brake pad composition varies both geographically, and with time, so differences between locations are not surprising. Sb was not detected in disc brake pads used by several Japanese manufacturers, indicating substitution of Sb sulphides by Sn sulphides (Faullant, 2002). On January 21, 2015, EPA, states, and the automotive industry signed an agreement to reduce the use of Cu and other materials in motor vehicle brake pads. The agreement calls for reducing Cu in brake pads to < 5% by weight in 2021 and 0.5% by 2025. Thus, attention should be given to the Cu/Sb ratio, as this will change in future source apportionment studies.

To derive chemical profiles for brake wear emissions in Europe, Hulskotte et al. (2014) analysed 65 brake pads and 12 brake discs. A mean Fe/Cu ratio of 2.0 was obtained for brake pads, whilst the brake disc wear samples were composed almost exclusively of Fe and thus very high ratios were observed. It was concluded that, under real life conditions, the Fe/Cu ratio can vary significantly, depending not only on the brake formulations, but also on the proportion of wear between discs and pads, as well as on the driving conditions. In the present work, the Fe/Cu ratios ranged from 22 to 68, averaging 35. The maximum value was registered in the cobbled road of the outskirts before washing. Higher ratios have been documented for other cities (Table 3).

Some researchers have reported high Zn/Sb values, ranging from 23 to 7,000, for tyre-related particles (Hjortenkrans et al., 2007; Kreider et al., 2010) and lower values (Zn/Sb < 25) for brake wear particles (Gietl et al., 2010; Hjortenkrans et al., 2007). In the present study, this ratio ranged from 8.4 to 66. The lowest value was registered in road dust from street # 5 (Av. 25 de Abril), where the steep exit to a residential neighbourhood contributes to particles enriched in Sb from brake wear. The highest ratio was obtained in the cobble street # 1, located on the outskirts of the city, showing samples of road dust more enriched in tyre wear components.

The Fe/Al ratio ranged from 0.32, in the most peripheral street with more rural characteristics, to 1.7 in the street next to the shipyards. The highest values were recorded in the streets with more traffic and braking. The same trends were observed for K/Al, Ca/Al and Ti/Al, for which values above those of the upper Earth's crust were generally found. Fe/Al, K/Al, Ca/Al and Ti/Al ratios in the upper crust of 0.40, 0.37, 0.38 and 0.04, respectively, have been documented (Wedepohl, 1995).

Table 3. Ratios between elements in inhalable sizes of road dust from different regions (n.a. – not available)

Ratios	This study	Alves et al. (2018)	Ramírez et al. (2019)		Pant et al. (2015)		Chen et al. (2012)	Wang et al. (2005)		Amato et al. (2009a)	
	Viana do Castelo	Oporto	Bogota (residential)	Bogota (commercial)	Birmingham	New Delhi	Beijing	Taiwan Hsinchu Downtown	Taiwan Freeway Tunnel	Barcelona City centre	Barcelona Ring roads
Fe/Al	0.96	1.75	0.41	0.54	0.85	0.78	0.57	0.77	0.85	1.21	0.94
K/Al	0.27	0.40	0.11	0.15	n.a.	n.a.	0.08	0.34	0.30	0.33	0.36
Ca/Al	0.51	1.02	0.95	0.72	0.37	1.26	2.23	0.37	0.62	3.05	2.73
Ti/Al	0.10	0.05	0.06	0.06	<0.01	0.01	0.02	n.a.	n.a.	0.07	0.07
Cu/Sb	17.7	11.1	10.2	8.29	5.0	16.0	n.a.	5.59	12.5	6.96	7.56
Zn/Sb	27.3	14.6	40.6	26.3	10.1	68	n.a.	22.9	99.2	7.67	12.3
Fe/Cu	35.1	49.3	n.a.	n.a.	211	194	182	0.27	0.22	37.2	52.1

The minimum, maximum and mean values of I_{geo} and PI for each element are shown in Table 4. Lithophile elements (e.g. Al, Ca, K, Mg and Na) fell into class 1, showing no contamination. On the other hand, as suggested by the enrichment factor, it was observed that road dust of the study region is extremely contaminated by elements from tyre and brake wear, such as Sb, Sn, Cu, and Zn. Extreme contamination was also noticed for Bi. The highest I_{geo} (7.9) and PI (367) values for this chemical element were found in PM_{10} from street #5, where the steep exit to a residential neighbourhood requires braking. Road dust samples were heavily to extremely contaminated by As, as well. Arsenic is used in alloys of lead (e.g. car batteries), and in the processing of glass, pigments, textiles, paper, metal adhesives and semiconductor electronic devices. Arsenic and its compounds, particularly the trioxide, are used in the production of pesticides, treated wood products, herbicides, and insecticides. The peak I_{geo} and PI values for As were found in samples from the street located in a residential area on the outskirts of the city. While one side of the street consists of terraced houses, the other side is flanked by a farm, where the use of agricultural chemicals may contribute to the accumulation of As in road dust. Background concentrations in soils have been reported to range from 1 to 40 mg kg^{-1}, with a mean value of 5 mg kg^{-1} (WHO, 2001), but a value of 165 mg kg^{-1} was obtained in the thoracic fraction of road dust of this street. The second highest concentration (145 mg kg^{-1}) was registered within the campus of the School of Technology and Management, behind which there are fields of corn and potatoes. Tarvainen et al. (2013) documented As concentrations for the <2 mm fraction of soil samples from agricultural (Ap horizon, 0-20 cm) and grazing land (Gr, 0-10 cm), covering western Europe. Median As concentrations were 5.7 mg kg^{-1}, for the Ap samples and 5.8 mg kg^{-1} for the Gr samples. The median As concentration in the agricultural soils of southern Europe was found to be more than 3-fold higher than in those of northern Europe. The majority of As anomalies were linked to mineral belts or ore deposits. Coal is another known source of arsenic (Yudovich and Ketris, 2005). However, the geology of Viana do Castelo is granitic, there are no coal ores, nor use of this fuel for thermoelectric production or in the domestic sector. Thus, the high levels of As in road dust of some streets are likely related to the nearby agricultural activities.

The integrated pollution load index (PLI) ranged from 2.8 (moderately polluted) to 6.3 (very highly polluted). Based on this parameter, half of the sampled streets were classified as moderately to highly polluted. PLI values (aggregate of six heavy metals) of 3.65, 2.76, 1.68, 1.53 and 1.25 were obtained in street dusts (fraction passing a 2 mm sieve) in commercial, high traffic, industrial, urban park, and residential areas of Zahedan, Iran, respectively (Kamani et al., 2015). Based on the same six heavy metals (Zn, Ni, Cd, Cr, Cu and Pb), integrated pollution levels from high to extremely high (1.22 to 13.1) were estimated for street dust samples collected from the central area of Tehran (Kamani et al., 2016). Based on the analysis of 10 elements in urban road dust samples below 2 mm (URD) from two populated agglomerations in Poland, geometric mean PLI values of 1.79 and 0.67 were determined for Katowice and Wrocław, respectively, showing the influence of abandoned industrial companies and coal-fired houses on the higher pollution levels in the first city (Rybak et al., 2020).

521

522 Table 4. Geoaccumulation and pollution indices for single elements in road dust samples

	I_{geo}				PI			
Elements	min	max	avg	contamination	min	max	avg	contamination
Al	-2.0	0.2	-1.0	uncontaminated	0.4	1.7	0.9	uncontaminated
Ca	-5.4	0.2	-1.7	uncontaminated	0.0	1.8	0.8	uncontaminated
Fe	-0.8	1.2	0.0	uncont. to moderate	0.8	3.4	1.7	moderate
K	-2.7	-0.1	-1.4	uncontaminated	0.2	1.4	0.7	uncontaminated
Mg	-3.2	-1.2	-2.1	uncontaminated	0.2	0.7	0.4	uncontaminated
Na	-3.2	-1.3	-2.5	uncontaminated	0.2	0.6	0.3	uncontaminated
P	-0.1	1.8	1.0	uncont. to moderate	1.4	5.1	3.3	considerable
S	-0.1	4.2	1.7	moderate	1.4	28.5	7.9	very high
Li	1.9	3.6	2.7	moderate to heavy	5.5	18.7	10.5	very high
Be	-0.4	1.4	0.5	uncont. to moderate	0.0	4.0	1.1	moderate
Sc	0.0	2.2	0.9	uncont. to moderate	1.5	6.8	3.2	considerable
Ti	-0.5	1.4	0.3	uncont. to moderate	1.1	3.9	2.0	moderate
V	-0.4	1.4	0.3	uncont. to moderate	1.2	3.9	2.0	moderate
Cr	2.4	3.9	3.1	heavy	0.0	21.8	8.4	very high
Mn	-0.5	1.3	0.3	uncont. to moderate	1.1	3.6	2.0	moderate
Co	-2.1	0.8	-0.2	uncontaminated	0.4	2.6	1.6	moderate
Ni	1.2	3.5	2.4	moderate to heavy	0.0	17.1	5.9	considerable
Cu	4.8	7.8	6.1	extreme	43.1	327	127	extreme
Zn	3.6	5.6	4.6	heavy to extreme	0.0	73.5	36.4	extreme
Ga	-0.4	1.7	0.5	uncont. to moderate	1.1	4.9	2.4	moderate
Ge	-1.1	3.6	1.3	moderate	0.7	17.6	5.6	considerable
As	3.8	5.8	4.9	heavy to extreme	20.5	82.4	50.1	extreme
Se	5.1	7.9	6.2	extreme	0.0	353	85.3	extreme
Rb	0.2	2.1	1.1	moderate	1.7	6.2	3.5	considerable
Sr	-2.6	0.1	-0.9	uncontaminated	0.3	1.6	0.9	uncontaminated
Y	-1.6	0.5	-0.5	uncontaminated	0.5	2.1	1.2	moderate
Zr	-1.8	0.5	-0.6	uncontaminated	0.0	2.2	1.0	moderate
Nb	-1.1	0.5	-0.3	uncontaminated	0.7	2.2	1.3	moderate
Mo	5.5	9.0	7.2	extreme	0.0	782	106	extreme
Cd	3.9	7.3	5.6	extreme	0.0	232	31.8	extreme
Sn	4.9	7.7	6.1	extreme	45.3	313	126	extreme
Sb	5.7	9.9	7.6	extreme	76.4	1398	435	extreme
Cs	1.1	2.8	1.9	moderate	3.1	10.3	6.1	very high
Ba	-0.5	2.7	1.2	moderate	1.1	10.1	4.1	considerable
La	-1.0	1.5	0.1	uncont. to moderate	0.7	4.3	1.8	moderate
Ce	-1.1	1.4	-0.1	uncontaminated	0.7	4.0	1.7	moderate

Pr	-0.5	1.8	0.5	uncont. to moderate	0.0	5.3	1.9	moderate
Nd	-0.8	1.6	0.2	uncont. to moderate	0.8	4.6	2.0	moderate
Sm	0.2	2.4	1.3	moderate	1.7	7.8	4.1	considerable
Gd	0.5	3.0	1.8	moderate	2.1	11.9	6.1	very high
Dy	-0.6	1.3	0.4	uncont. to moderate	1.0	3.8	2.2	moderate
Er	-0.60	0.8	0.2	uncont. to moderate	0.0	2.6	0.7	uncontaminated
Yb	0.1	1.4	0.8	uncont. to moderate	0.0	4.1	1.1	moderate
Hf	-1.3	0.6	-0.4	uncontaminated	0.0	2.2	1.1	moderate
W	3.0	5.6	3.8	heavy	0.0	71.2	20.0	extreme
Tl	0.7	1.9	1.3	moderate	0.0	5.6	1.0	moderate
Pb	2.1	4.4	3.2	heavy	6.4	32.1	16.2	extreme
Bi	5.6	7.9	6.8	extreme	0.0	367	161	extreme
Th	-0.3	2.1	0.7	uncont. to moderate	1.2	6.6	2.8	moderate
U	1.8	3.3	2.7	moderate to heavy	5.1	15.0	10.5	very high

Note: Cr, Ni, and Se detected only in samples from 5 roads, Er and Yb in samples from 3 roads, Mo, Cd and Tl in samples from 2 roads

E_{i_r} indicated the very high risk posed by Sb, Cd, Cu and As (Fig. 2). On average, a global RI value of 5316 was obtained, indicating that the thoracic fraction of road dust of Viana do Castelo may pose a significantly high potential ecological risk, and management procedures should be adopted. Sb can be regarded as the pollutant of highest concern, since it represented 57.3% of RI. Cd, Cu, As and Pb accounted for 18.0, 11.9, 9.4 and 1.5% of the potential ecological risk, respectively, while the contribution from other elements was low. RI values ranging from 82 to 50 (mean value of 234) have been reported for Tehran, with Cd representing a considerable potential ecological risk (Kamani et al., 2016). In Eslamshahr, another Iranian city, the highest monomial E_{i_r} values, ranging from 33.3 to 153, were also observed for Cd (Kamani et al., 2018). In road dust < 100 μm collected in Beihai and Shanghai, China, the E_{i_r} values indicated the low risk posed by all metals. However, the ecological index in Beihai highlighted the considerable (E_{i_r} = 149) and high (E_{i_r} = 254) risks for Hg and Ni, respectively (Chen et al. (2019). In Lublin, Poland, the determination of Cd, Cr, Cu, Ni, Pb and Zn in street dust (< 63 μm) collected in 2018 indicated a moderate ecological risk for 84% of the samples, while the remaining 16% were assigned to the "considerable" class. Cd was the element with the strongest influence on the level of this index (Zgłobicki et al., 2019).

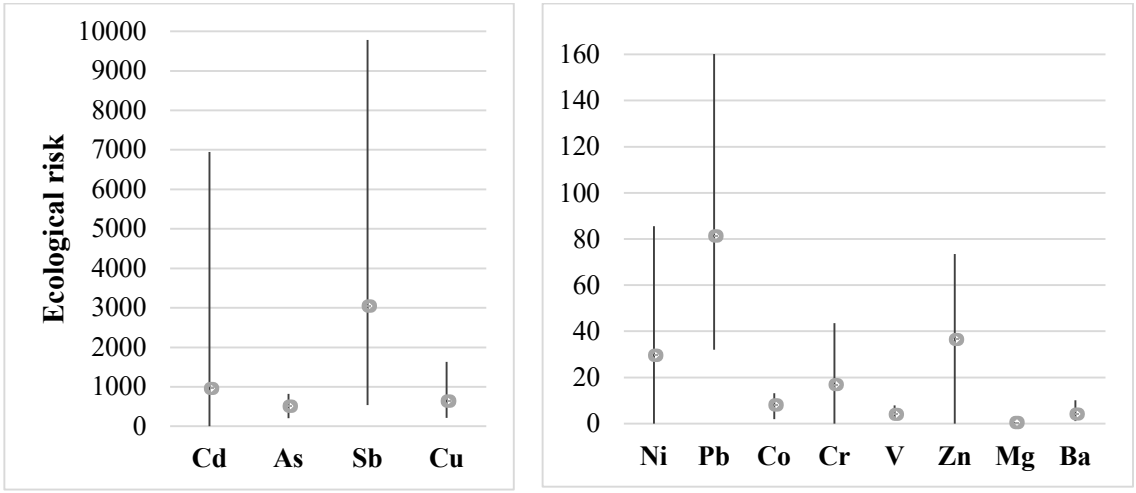

Fig. 2. Potential ecological risk factors of individual elements (E_{r_i}) in road dust samples (minimum, maximum and mean values)

Human health risk

For some elements, the hazard index was higher than the safe value of 1 for both children and adults (Fig. 3). Li, V, Mn, Co, Zn, Sr, Sn, Ba and U presented HI values much lower than 1, thus suggesting that there were no significant non-carcinogenic risks to the public posed by these elements. The HI values for adults were approximately an order of magnitude lower than those for children. Therefore, children are potentially more susceptible to the health effects from exposure to metals in road dust. In some streets, the non-carcinogenic risk for children due to multiple elements is worrying, reaching HI values up to 65 (Zr), 11 (Sb), 5.5 (As), Cr (2.8), 2.2 (Mo), 1.6 (Pb), 1.5 (Fe) and 1.2 (Cu). The maximum values for Zr, Sb, Cr, Fe and Cu were obtained in samples from the street with a steep exit to a residential neighbourhood (street # 5), more prone to brake and tyre wear. The highest HI for As was registered in the street most impacted by agricultural activities.

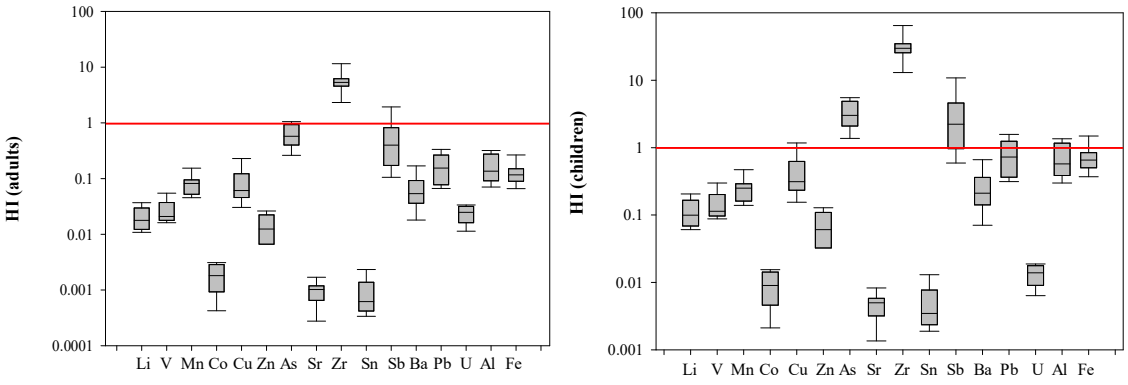

Fig. 3. Non-carcinogenic risk (hazard index, HI) estimated for adults and children due to metals in road dust particles

The carcinogenic effects of Co, Cr, Ni, Cd and As were assessed through the inhalation exposure route only, owing to the shortage of SF values for the ingestion and dermal pathways. The total carcinogenic risks were all lower than 1×10^{-6}, except for road dust samples collected in street # 5, where a TCR value of 1.88×10^{-6} was obtained. These results indicate that, in general, the total cancer risk can be considered insignificant. However, in street # 5, the CR for Cr (1.84×10^{-6}), slightly exceeding the reference value, indicates potential carcinogenic risk in that sampling site.

Conclusions

Loadings and chemical patterns of inhalable road dust particles were investigated in a Southern European city. Since it has been shown that emission inventories and source apportionment methodologies should employ databases obtained locally, this study has the potential to contribute to new emission factors and chemical fingerprints to more accurately quantify the contribution of road dust resuspension to atmospheric levels.

Various geochemical indices were applied to the datasets to assess the degree of contamination. While minimal enrichments factors were always observed for elements such as Mg, Na and K, very or extremely high factors were registered for Cu, Zn, Sn, Sb, As, Se and Bi, reflecting the substantial environmental pollution caused by anthropogenic sources. The geochemical and pollution indices revealed that road dust of the study region is extremely contaminated by elements from tyre and brake wear. The highest contamination degrees were observed in a street where the steep exit to a residential neighbourhood requires braking. Road dust samples were also heavily to extremely contaminated by As, especially in the streets more impacted by agriculture activities. The integrated pollution load index ranged from 2.8 (moderately polluted) to 6.3 (very highly polluted). A very high ecological risk factor for multiple metals of 5316 was obtained, 57% of which was due to the contribution of Sb. Thus, brake wear represents a noteworthy input to the thoracic fraction of road dust of Viana do Castelo, and together with other traffic related emissions, may pose a significantly high potential ecological risk.

Although the total cancer risk was found to be insignificant for both children and adults, the assessment of non-carcinogenic health hazards of exposure to heavy metals indicated that the daily doses, especially due to hand to mouth ingestion of road dust particles, exceeded the reference values. Thus, exposure to elements such as Zr, Sb, As, Cr, Mo, Pb, Fe and Cu may trigger neurological and developmental disorders, and the heavy metals may accumulate in the body for a long time. The hazards of exposure to road dust cannot be overlooked, and the ecological and health implications require further detailed investigation. Additionally, preventive and corrective actions should be targeted.

Credit authorship contribution statement

Célia Alves: Funding acquisition, Project administration, Conceptualisation, Supervision, Data curation, Investigation, Formal analysis, Writing - original draft. **Estela D. Vicente**: Investigation, Formal analysis. **Ana M.P. Vicente:** Investigation. **Ismael Casotti Rienda**: Investigation, Data curation. **Mário Tomé**: Investigation. **Xavier Querol:** Investigation. **Fulvio Amato:** Conceptualisation, Validation, Writing - review & editing.

Declaration of competing interest

The authors declare that they have no known competing financial interests or personal relationships that may have influenced the present study.

Acknowledgments

This work was financially supported by the project "Chemical and toxicological SOurce PROfiling of particulate matter in urban air (SOPRO)", POCI-01-0145-FEDER-029574, funded by FEDER, through Compete2020 - *Programa Operacional Competitividade e Internacionalização* (POCI), and by national funds (OE), through FCT/MCTES. An acknowledgement is also given to the Portuguese Foundation of Science and Technology (FCT) and to the POHP/FSE funding programme for the fellowship SFRH/BD/117993/2016. Ana Vicente is subsidised by national funds (OE), through FCT, I.P., in the scope of the framework contract foreseen in the numbers 4, 5 and 6 of Article 23, of the Decree-Law 57/2016, of August 29, changed by Law 57/2017, of July 19. Moreover, thanks are due for the financial support to CESAM (UIDB/50017/2020+UIDP/50017/2020), to FCT/MCTES through national funds, and co-funding by FEDER, within the PT2020 Partnership Agreement and Compete 2020. We are grateful to the Viana do Castelo City Council, and especially to Ricardo Carvalhido, for all the logistic support.

References

Adimalla, N., 2020. Heavy metals contamination in urban surface soils of Medak province, India, and its risk assessment and spatial distribution. Environ. Geochem. Health 42, 59-75.

Alves, C.A., Evtyugina, M., Vicente, A.M.P., Vicente, E.D., Nunes, T.V., Silva, P.M.A., Duarte, M.A.C., Pio, C.A., Amato, F., Querol, X., 2018. Chemical profiling of PM_{10} from urban road dust. Sci. Total Environ. 634, 41-51.

632 Alves, C.A., Vicente, A.M., Calvo, A.I., Baumgardner, D., Amato, A., Querol, X., Pio, C., Gustafsson,
633 M. 2020. Physical and chemical properties of non-exhaust particles generated from wear between
634 pavements and tyres. Atmos. Environ. 224, 117252.
635 Amato, F., Alastuey, A., de la Rosa, J., Gonzalez Castanedo, Y., Sánchez de la Campa, A.M., Pandolfi,
636 M., Lozano, A., Contreras González, J., Querol, X., 2014. Trends of road dust emissions
637 contributions on ambient air particulate levels at rural, urban and industrial sites in southern Spain.
638 Atmos. Chem. Phys. 14, 3533-3544.
639 Amato, F., Alastuey, A., Karanasiou, A., Lucarelli, F., Nava, S., Calzolai, G., Severi, M., Becagli, S.,
640 Gianelle, V.L., Colombi, C., Alves, C., Custódio, D., Nunes, T., Cerqueira, M., Pio, C., Eleftheriadis,
641 K., Diapouli, E., Reche, C., Minguillon, M.C., Manousakas, M.I., Maggos, T., Vratolis, S., Harrison,
642 R.M., Querol, X., 2016a. AIRUSE-LIFE plus: a harmonized PM speciation and source
643 apportionment in five southern European cities. Atmos. Chem. Phys. 16, 3289-3309.
644 Amato, F., Bedogni, M., Padoan, E., Querol, X., Ealo, M., Rivas, I., 2017. Characterization of road dust
645 emissions in Milan: Impact of vehicle fleet speed. Aerosol and Air Qual. Res. 17, 2438-2449.
646 Amato, F., Favez, O., Pandolfi, M., Alastuey, A., Querol, X., Moukhtar, S., Bruge, B., Verlhac, S.,
647 Orza, J.A.G., Bonnaire, N., Le Priol, T., Petit, J.-F., Sciare, J., 2016b. Traffic induced particle
648 resuspension in Paris: emission factors and source contributions. Atmos. Environ. 129, 114-124.
649 Amato, F., Pandolfi, M., Moreno, T., Furger, M., Pey, J., Alastuey, A., Bukowiecki, N., Prévôt, A.S.H.,
650 Baltensperger, U., Querol, X., 2011. Sources and variability of inhalable road dust particles in three
651 European cities. Atmos. Environ. 45, 6777-6787.
652 Amato, F., Pandolfi, M., Viana, M., Querol, X., Alastuey, A., Moreno, T., 2009a. Spatial and chemical
653 patterns of PM_{10} in road dust deposited in urban environment. Atmos. Environ. 43, 1650-1659.
654 Amato, F., Querol, X., Alastuey, A., Pandolfi, M., Moreno, T., Gracia, J., Rodriguez, P., 2009b.
655 Evaluating urban PM_{10} pollution benefit induced by street cleaning activities. Atmos. Environ. 43,
656 4472-4480.
657 Amato, F., Querol, X., Johansson, C., Nagl, C., Alastuey, A., 2010. A review on the effectiveness of
658 street sweeping, washing and dust suppressants as urban PM control methods. Sci. Total Environ.
659 408, 3070-3084.
660 Brines, M., Dall'Osto, M., Amato, F., Minguillón, M.C., Karanasiou, A., Alastuey, A., Querol, X.,
661 2016. Vertical and horizontal variability of PM_{10} source contributions in Barcelona during SAPUSS.
662 Atmos. Chem. Phys. 16, 6785–6804.
663 Cai, K., Li, C., 2019. Street dust heavy metal pollution source apportionment and sustainable
664 management in a typical city -Shijiazhuang, China. Int. J. Environ. Res. Public Health 16, 2625.
665 http://dx.doi.org/10.3390/ijerph16142625
666 Casal, C.S., Arbilla, G., Corrêa, S.M., 2014. Alkyl polycyclic aromatic hydrocarbons emissions in
667 diesel/biodiesel exhaust. Atmos. Environ. 96, 107-116.

668 Chang, Y., Chou, C., Su, K., Tseng, C., 2005. Effectiveness of street sweeping and washing for
669 controlling ambient TSP. Atmos. Environ. 39, 1891-1902.
670 Chen, H., Teng, Y., Lu, S., Wang, Y., Wang, J., 2015. Contamination features and health risk of soil
671 heavy metals in China. Sci. Total Environ. 212-213, 143-153.
672 Chen, J., Wang, W., Liu, H., Ren, L. 2012. Determination of road dust loadings and chemical
673 characteristics using resuspension. Environ. Monit. Assess. 184, 1693-1709.
674 Chen, X., Guo, M., Feng, J., Liang, S., Han, D., Cheng, J., 2019. Characterization and risk assessment
675 of heavy metals in road dust from a developing city with good air quality and from Shanghai, China.
676 Environ. Sci. Pollut. Res. 26, 11387-11398.
677 Chou, C.M., Chang, Y.M., Lin, W.Y., Tseng, C.H., Chen, L., 2007. Evaluation of street sweeping and
678 washing to reduce ambient PM_{10}. Int. J. Environ. Pollut. 31, 431-448.
679 Denier van der Gon, H.A.C., Gerlofs-Nijland, M.E., Gehring, R., Gustafsson, M., Janssen, N., Harrison,
680 R.M., Hulskotte, J., Johansson, C., Jozwicka, M., Keuken, M., Krijgsheld, K., Ntziachristos, L.,
681 Riediker, M., Cassee, F.R., 2013. The policy relevance of wear emissions from road transport, now
682 and in the future e an international workshop report and consensus statement. J. Air Waste Manag.
683 Assoc. 63, 136-149.
684 Dong, S., Ochoa, R., Harrison, R.M., Greene, D., North, R., Fowler, G., Weiss, D., 2017. Isotopic
685 signatures suggest important contributions from recycled gasoline, road dust and non-exhaust traffic
686 sources for copper, zinc and lead in PM_{10} in London, United Kingdom. Atmos. Environ. 165, 88-98.
687 Faullant, P., 2002. Particle size effects of tin sulfides in disc brake pads. SAE Int.
688 http://dx.doi.org/10.4271/2002-01-2591
689 Font, A., Fuller, G.W., 2016. Did policies to abate atmospheric emissions from traffic have a positive
690 effect in London? Environ. Pollut. 218, 463-474.
691 Gietl, J., Lawrence, R., Thorpe, A., Harrison, R., 2010. Identification of brake wear particles and
692 derivation of a quantitative tracer for brake dust at a major road. Atmos. Environ. 44, 141–146.
693 Grigoratos, T., Martini, G., 2015. Brake wear particle emissions: a review. Environ. Sci. Pollut. Res.
694 22, 2491-2504.
695 Guevara, M., 2016. Emissions of Primary Particulate Matter. In: Airborne Particulate Matter: Sources,
696 Atmospheric Processes and Health, Vol. 42, Harrison R.M., Hester R.E., Querol X. (Eds.). Royal
697 Society of Chemistry, Cambridge, UK, pp.1-34.
698 Gulia, S., Goyal, P., Goyal, S.K., Kumar, R., 2019. Re-suspension of road dust: contribution,
699 assessment and control through dust suppressants - a review. Int. J. Environ. Sci. Technol. 16, 1717-
700 1728.
701 Gustafsson, M., Blomqvist, G., Gudmundsson, A., Dahl, A., Jonsson, P., Swietlicki, E., 2009. Factors
702 influencing PM_{10} emissions from road pavement wear. Atmos. Environ. 43, 4699-4702.

703 Gustafsson, M., Blomqvist, G., Järlskog, I., Lundberg, J., Janhäll S., Elmgren M., Johansson C.,
704 Norman M., Silvergren S., 2019. Road dust load dynamics and influencing factors for six winter
705 seasons in Stockholm, Sweden. Atmos. Environ. X 2, 100014.
706 Harrison, R.M., Jones, A.M., Gietl, J., Yin, J., Green, D.C., 2012. Estimation of the contributions of
707 brake dust, tire wear, and resuspension to nonexhaust traffic particles derived from atmospheric
708 measurements. Environ. Sci. Technol. 46, 6523-6529.
709 Hjortenkrans, D., Bergback, B., Haggerud, A., 2007. Metal emissions from brake linings and tires: case
710 studies of Stockholm, Sweden 1995/1998 and 2005. Environ. Sci. Technol. 41, 5224–5230.
711 Hooftman, N., Oliveira, L., Messagie, M., Coosemans, T., Mierlo, J.V., 2016. Environmental analysis
712 of petrol, diesel and electric passenger cars in a Belgian urban setting. Energies 9, 84.
713 http://dx.doi.org/10.3390/en9020084
714 Hosiokangas, J., Vallius, M., Ruuskanen, J., Mirme, A., Pekkanen, J., 2004. Resuspended dust episodes
715 as an urban air-quality problem in subarctic regions. Scand. J. Work Environ. Health 30, suppl 2,
716 28-35.
717 Hulskotte, J.H.J., Roskam, G.D., Denier van der Gon, H.A.C., 2014. Elemental composition of current
718 automotive braking materials and derived air emission factors. Atmos. Environ. 99, 436-445.
719 Jazcilevich, A., Wellens, A., Siebe, C., Rosas, I., Bornstein, R., Riojas-Rodríguez, H., 2012. Application
720 of a stochastic vehicular wake erosion model to determine $PM_{2.5}$ exposure. Aeolian Res. 4, 31–37.
721 Kalaiarasan, G., Balakrishnan, R.M., Sethunath, N.A., Manoharan, S., 2018. Source apportionment
722 studies on particulate matter (PM_{10} and $PM_{2.5}$) in ambient air of urban Mangalore, India. J. Environ.
723 Manage. 217, 815-824.
724 Kamani, H., Ashrafi, S.D., Isazadeh, S., Jaafari, J., Hoseini, S., Mostafapour, F.K., Bazrafshan, E.,
725 Nazmara, S., Mahvi, A.H., 2015. Heavy metal contamination in street dusts with various land uses
726 in Zahedan, Iran. Bull. Environ. Contam. Toxicol. 94, 382-386.
727 Kamani, H., Mahvi, A.H., Seyedsalehi, M., Jaafari, J., Hoseini, M., Safari, G.H., Dalvand, A., Aslani,
728 H., Mirzaei, N., Ashrafi, S.D., 2017. Contamination and ecological risk assessment of heavy metals
729 in street dust of Tehran, Iran. Int. J. Environ. Sci. Technol. 14, 2675-2682.
730 Kamani, H., Mirzaei, N., Ghaderpoori, M., Bazrafshan, E., Rezaei, S., Mahvi, A.H., 2018.
731 Concentration and ecological risk of heavy metal in street dusts of Eslamshahr, Iran. Hum. Ecol.
732 Risk Assess. 4, 961-970.
733 Karagulian, F., Belis, C.A., Dora, C.F.C., Prüss-Ustün, A.M., Bonjour, S., Adair-Rohani, H., Amann,
734 M., 2015. Contributions to cities' ambient particulate matter (PM): A systematic review of local
735 source contributions at global level. Atmos. Environ. 120, 475-483.
736 Karanasiou, A., Moreno, T., Amato, F., Lumbreras, J., Narros, A., Borge, R., Tobías, A., Boldo, E.,
737 Linares, C., Pey, J., Reche, C., Alastuey, A., Querol, X., 2011. Road dust contribution to PM levels
738 – Evaluation of the effectiveness of street washing activities by means of Positive Matrix
739 Factorization. Atmos. Environ. 2193-2201.

Ketzel, M., Omstedt, G., Johansson, C., Düring, I., Pohjola, M., Oettl, D., Gidhagen, L., Wåhlina, P., Lohmeyer, A., Haakana, M., Berkowicz, R., 2007. Estimation and validation of $PM_{2.5}/PM_{10}$ exhaust and non-exhaust emission factors for practical street pollution modelling. Atmos. Environ. 41, 9370-9385.

Khan, R.K., Strand, M.A., 2018. Road dust and its effect on human health: a literature review. Epidemiol. Health 40, Article ID: e2018013. https://doi.org/10.4178/epih.e2018013

Klöckner, P., Reemtsma, T., Eisentraut, P., Braun, U., Ruhl, S.A., Wagner, S., 2019. Tire and road wear particles in road environment – Quantification and assessment of particle dynamics by Zn determination after density separation. Chemosphere 222, 714-721.

Kreider, M., Panko, J., McAtee, B., Sweet, L., Finley, B., 2010. Physical and chemical characterization of tire-related particles: comparison of particles generated using different methodologies. Sci. Total Environ. 408, 652–659.

Lawrence, S., Sokhi, R., Ravindra, K., Mao, H., Prain, H.D., Bull, I.D., 2013. Source apportionment of traffic emissions of particulate matter using tunnel measurements. Atmos. Environ. 77, 548-557.

Mostoni, S., Milana, P., Di Credico, B., D'Arienzo, M., Scotti, R., 2019. Zinc-based curing activators: New trends for reducing zinc content in rubber vulcanization process. Catalysts 9, 664. https://doi.org/10.3390/catal9080664

Österle, W., Dmitriev, A.I., 2016. The role of solid lubricants for brake friction materials. Lubr. 4. https://doi.org/10.3390/lubricants4010005

Padoan, E., Amato, F., 2018. Vehicle Non-Exhaust Emissions: Impact on Air Quality. In: Non-Exhaust Emissions: An Urban Air Quality Problem for Public Health - Impact and Mitigation Measures, Amato F. (Ed.). Academic Press, London, UK, pp.21-65.

Pant, P., Baker, S.J., Shukla, A., Maikawa, C., Pollitt, K.J.G., Harrison, R.M., 2015. The PM_{10} fraction of road dust in the UK and India: Characterization, source profiles and oxidative potential. Sci. Total Environ. 530-531, 445-452.

Pant, P., Harrison, R.M., 2013. Estimation of the contribution of road traffic emissions to particulate matter concentrations from field measurements: A review. Atmos. Environ. 77, 78-97.

Penkała, M., Ogrodnik, P., Rogula-Kozłowska, W., 2018. Particulate matter from the road surface abrasion as a problem of non-exhaust emission control. Environments 5, 9. https://doi.org/10.3390/environments5010009

Ramírez, O., Sánchez de la Campa, A.M., Amato, F., Moreno, T., Silva, L.F., de la Rosa, J.D., 2019. Physicochemical characterization and sources of the thoracic fraction of road dust in a Latin American megacity. Sci. Total Environ. 652, 434-446.

Rybak, J., Wróbel, M., Bihałowicz, J.S., Rogula-Kozłowska, W., 2020. Selected metals in urban road dust: Upper and Lower Silesia case study. Atmosphere 11, 290. https://doi.org/10.3390/atmos11030290

777 Sanderson, R.T., 2019. Bismuth. Encyclopædia Britannica. Encyclopædia Britannica, Inc.
778 https://www.britannica.com/science/bismuth
779 Thorpe, A.J., Harrison, R.M., Boulter, P.G., McCrae, I.S., 2007. Estimation of particle resuspension
780 source strength on a major London road. Atmos. Environ. 41, 8007-8020.
781 Timmers, V.R.J.H., Achten, P.A.J., 2016. Non-exhaust PM emissions from electric vehicles. Atmos.
782 Environ. 134, 10-17.
783 Vogelsang, C., Lusher, A.L., Dadkhah, M.E., Sundvor, I., Umar, M., Ranneklev ,S.B., Eidsvoll, D.,
784 Meland, S., 2019. Microplastics in road dust – characteristics, pathways and measures. Norwegian
785 Institute for Water Research – NIVA. Report no. 7361-2019. Oslo, Norway.
786 von Uexküll, O., Skerfving, S., Doyle, R., Braungart, M., 2005. Antimony in brake pads-a carcinogenic
787 component? J. Clean. Prod. 13,19-31.
788 Wang, C.F., Chang, C.Y., Tsai S.F., Chiang H.L., 2005. Characteristics of road dust from different
789 sampling sites in Northern Taiwan. J. Air Waste Manag. Assoc. 55, 1236-1244.
790 Wang, N., Wang, A., Kong, L., He, M., 2018. Calculation and application of Sb toxicity coefficient for
791 potential ecological risk assessment. Sci. Total Environ. 610–611, 167–174.
792 Wang, Z., Li, K., Lambert, P., Yang, C. 2007. Identification, characterization and quantitation of
793 pyrogenic polycylic aromatic hydrocarbons and other organic compounds in tire fire products. J.
794 Chromatogr. A 1139,14-26.
795 Watson, J.G., Chow, J.C., Pace, T.G., 2000. Fugitive dust emissions. In: Air Pollution Engineering
796 Manual, Second Edition, Davis W.T. (Ed.). John Wiley & Sons, Inc., New York, pp. 117-135.
797 Wedepohl, K.H., 1995. The composition of the continental crust. Geochim. Cosmochim. Acta 59, 1217-
798 1239.
799 Weinbruch, S., Worringen, A., Ebert, M., Scheuvens, D., Kandler, K., Pfeffer, U., Bruckmann, P., 2014.
800 A quantitative estimation of the exhaust, abrasion and resuspension components of particulate traffic
801 emissions using electron microscopy. Atmos. Environ. 99, 175-182.
802 Wen, H., Carignan, J., 2007. Reviews on atmospheric selenium: Emissions, speciation and fate. Atmos.
803 Environ. 41, 7151-7165.
804 WHO, 2001. Arsenic and Arsenic Compounds (Environmental Health Criteria 224), 2nd ed.;
805 International Programme on Chemical Safety. World Health Organization, Geneva, Switzerland.
806 WHO, 2016. Ambient air pollution: a global assessment of exposure and burden of disease. World
807 Health Organization. Geneva, Switzerland. http://www.who.int/iris/handle/10665/250141
808 Wik, A., Dave, G., 2009. Occurrence and effects of tire wear particles in the environment - a critical
809 review and an initial risk assessment. Environ. Pollut. 157, 1-11.
810 Wu, J., Teng, Y., Lu, S., Wang, Y., Jiao, X., 2014. Evaluation of soil contamination indices in a mining
811 area of Jiangxi, China. PLoS ONE 9(11), e112917. http://dx.doi.org/10.1371/journal.pone.0112917

812 Yang, J., Teng, Y., Song, L., Zuo, R., 2016. Tracing sources and contamination assessments of heavy
813 metals in road and foliar dusts in a typical mining city, China. PLoS One, 11, Article e0168528.
814 https://doi.org/10.1371/journal.pone.0168528
815 Yudovich Y.E., Ketris M.P., 2005. Arsenic in coal: a review. Int. J. Coal Geol. 61, 141-196.
816 Yu, L., Wang, G. Zhang, R., Zhang, L., Song, Y., Wu, B., Li, X., An, K., Chu, J., 2013. Characterization
817 and source apportionment of $PM_{2.5}$ in an urban environment in Beijing. Aerosol Air Qual. Res. 13,
818 574-583.
819 Zgłobicki, W., Telecka, M., Skupiński, S., 2019. Assessment of short-term changes in street dust
820 pollution with heavy metals in Lublin (E Poland) - levels, sources and risks. Environ. Sci. Pollut.
821 Res. 26, 35049-35060.
822 Zhang, J., Zhang, X., Wu, L., Wang, T., Zhao, J., Zhang, Y., Men, Z., Mao, H., 2018. Occurrence of
823 benzothiazole and its derivates in tire wear, road dust, and roadside soil. Chemosphere 201, 310-
824 317.
825

Loadings, chemical patterns and risks of inhalable road dust particles in an Atlantic city in the north of Portugal

Célia A. Alves[1*], Estela D. Vicente[1], Ana M.P. Vicente[1], Ismael Casotti Rienda[1], Mário Tomé[2], Xavier Querol[3], Fulvio Amato[3]

[1]Department of Environment, Centre for Environmental and Marine Studies, University of Aveiro, 3810-193 Aveiro, Portugal
[2]PROMETHEUS, School of Technology and Management (ESTG), Avenida do Atlântico, nº 644, 4900-348 Viana do Castelo, Portugal
[3]Institute of Environmental Assessment and Water Research, Spanish Research Council, 08034 Barcelona, Spain

SUPPLEMENTARY MATERIAL

• Meteorological information

Road dust sampling in Viana do Castelo was carried out in September and October 2018. The hourly average wind direction in this city throughout September is predominantly from the north. This direction represents approximately 50% of the total records. In October, the northern quadrant dominates until the middle of the month. The representativeness of this direction decreases in the second half, in which the prevailing winds blow from the south.

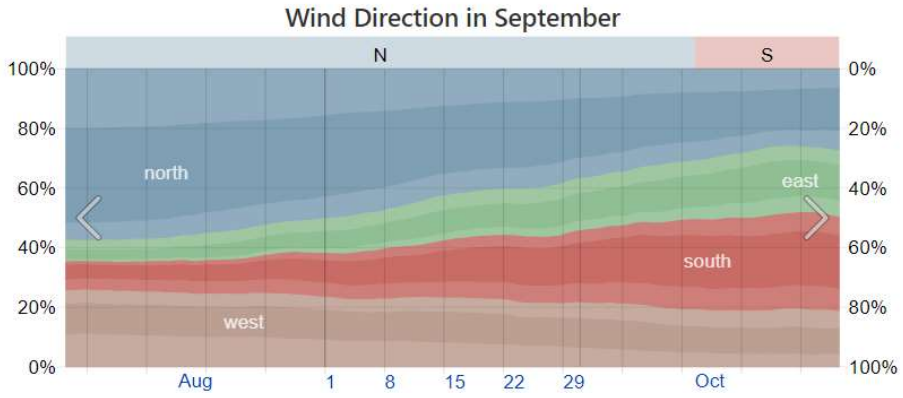

* Corresponding author. E-mail: celia.alves@ua.pt

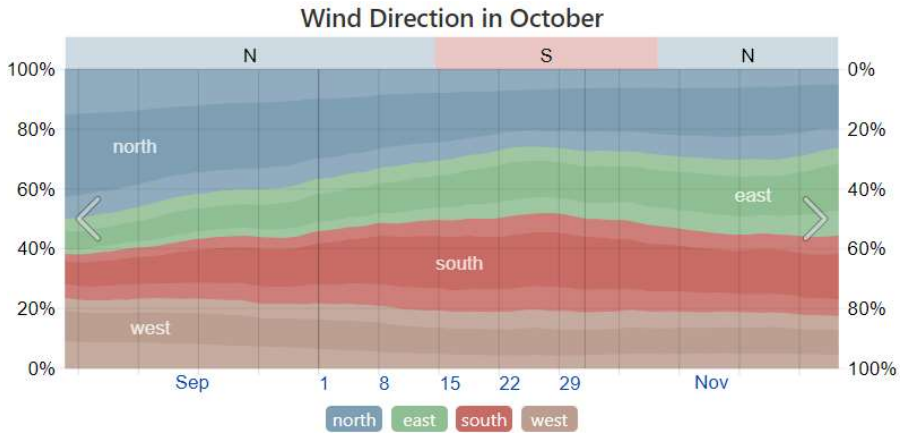

Fig. S1. Percentage of hours in which the mean wind direction is from each of the four cardinal directions. Hours in which the mean wind speed is lower than 1.0 mph were not included. The lightly tinted areas at the boundaries are the percentage of hours spent in intermediate directions (northeast, southeast, southwest, and northwest). Data source: Weather Spark.

- **Analytical methods**

Table S1. Internal standards used in the quantification of organic compounds

Internal Standards	**Quantification Ion (m/z)**
1,4-Dichlorobenzene-d4	150
Naphthalene-d8	136
Acenaphthene-d10	164
Fluorene-d10	176
Phenanthrene-d10	188
Chrysene-d12	240
Benzo[a]pyrene-d12	264
Perylene-d12	264
Diethyl phthalate-3,4,5,6-d4	153
Bis(2-ethylhexyl)phthalate-3,4,5,6-d_4	149
1-Chlorododecane	91
1-Chlorohexadecane	57
Tetracosane-d50	66

Table S2. Quantification ions for the determination of PAHs by GC-MS operated in the selected ion monitoring mode (SIM)

Rings	Compounds	Quantification Ion (m/z)
central benzene ring substituted with two phenyl groups	Terphenyl	230
2	Naphthalene	128
3	Acenaphthylene	152
3	Acenaphthene	153
3	Fluorene	166
3	Phenanthrene	178
3	Anthracene	178
4	Fluoranthene	202
4	Pyrene	202
4	Chrysene	228
4	Benzo[a]anthracene	228
5	Perylene	252
5	Benzo[b]fluoranthene	252
5	Benzo[k]fluoranthene	252
5	Benzo[a]pyrene	252
5	Dibenzo[a,h] anthracene	278
6	Indeno[1,2,3-cd]pyrene	276
6	Benzo[g,h,i]perylene	276

Table S3. Quantification ions for the determination of alkylated PAHs by GC-MS operated in the selected ion monitoring mode (SIM)

	Alkyl-PAHs	Quantification Ion (m/z)
	Retene	219
C1-naphthalenes	Methylnaphthalene	142
C2-naphthalenes	Dimethylnaphthalene	156
C1-fluorenes	Methylfluorene	180
C3-fluorenes	Trimethylfluorene	208
C1-phenanthrenes	Methylphenantrene	192
C2-phenanthrenes	Dimethylphenantrene	206
C3-phenanthrenes	Trimethylphenanthrene	220
C1-fluoranthenes/pyrenes	Methylfluoranthene/Methylpyrene	216
C3-dibenzothiophenes	Trimethyldibenzothiophene	226
Heterocyclic aromatics	Carbazole	167
	Benzothiazole	135

Table S4. Quantification ions for the determination of plasticisers by GC-MS operated in the selected ion monitoring mode (SIM)

Plasticisers	Quantification Ion (m/z)
Dimethyl phthalate	163
Diethyl phthalate	149
Di-n-butyl phthalate	149
Benzyl butyl phthalate	149
Bis(2-ethylhexyl) adipate	129
Bis(2-ethylhexyl) phthalate	149
Di-n-octyl phthalate	149
Diisononyl phthalate	149
Diisodecyl phthalate	149

Table S5. Definition and reference values of some parameters for health assessment of metal(loid)s in road dusts (Adimalla, 2020; and references therein)

Factor	Definition	Units	Adult	Children
IR_{ing}	Ingestion rate	mg day^{-1}	200	100
ED	Exposure duration	years	30	6
EF	Exposure frequency	days $year^{-1}$	365	365
CF	Conversion factor	kg mg^{-1}	1.00×10^{-6}	1.00×10^{-6}
BW	Body weight	kg	70	20
AT	Average time (non-carcinogenic)	years	365×ED	365×ED
	Average time (carcinogenic)	years	70×ED	70×ED
SA	Exposed skin surface area	cm^2	4350	1600
SAF	Skin adherence factor	mg cm^{-2}	0.7	0.2
DAF	Dermal absorption factor	–	0.001	0.001
IR_{inh}	Inhalation rate	m^3 day^{-1}	12.8	7.63
PEF	Particle emission factor	m^3 kg^{-1}	1.36×10^9	1.36×10^9

Table S6. Reference doses (R_fD) and slope factors (SF) for metal(loid)s (Adimalla, 2020; Faiz et al., 2012; Ferreira-Baptista and de Miguel, 2005; Li et al., 2017; Xu et al., 2015).

Metal	R_fD_{ing} (mg kg^{-1} day^{-1})	R_fD_{inh} (mg kg^{-1} day^{-1})	$\underline{R_fD_{dermal}}$ (mg kg^{-1} day^{-1})	SF (mg kg^{-1} day^{-1})
As	3.00×10^{-4}		1.23×10^{-4}	1.5×10^{0}
Zn	3.00×10^{-1}	3.00×10^{-1}	6.00×10^{-2}	
Cu	4.00×10^{-2}	4.02×10^{-2}	1.20×10^{-2}	
Pb	3.50×10^{-3}	3.52×10^{-3}	5.25×10^{-4}	
Cr	3.00×10^{-3}	2.86×10^{-5}	6.00×10^{-5}	4.20×10^{1}
Ni	2.00×10^{-2}	2.06×10^{-2}	5.40×10^{-3}	8.40×10^{-1}
Cd	1.00×10^{-3}	1.00×10^{-3}	1.00×10^{-5}	6.30×10^{0}
Mn	4.6×10^{-2}	1.43×10^{-5}	1.84×10^{-3}	
Fe	7.0×10^{-1}			
Sb	4.0×10^{-4}			
Al	1.00×10^{0}	1.43×10^{-3}	1.00×10^{-1}	
Co	2.0×10^{-2}	1.43×10^{-4}	4.9×10^{-3}	9.8×10^{0}
Ba	7.00×10^{-2}	1.43×10^{-4}	4.9×10^{-3}	
Mo	5.0×10^{-3}		1.9×10^{-3}	
Sr	6.0×10^{-1}		1.2×10^{-1}	
V	7.0×10^{-3}	7.0×10^{-3}	7.0×10^{-3}	

Table S7. Mutagenic and carcinogenic equivalency factors for PAHs (Błaszczyk et al., 2017; and references therein)

	Mutagenic equivalency factor (MEF)	Carcinogenic equivalency factor (TEF)
Naphthalene	-	0.001
Acenaphthene	-	0.001
Fluorene	-	0.001
Phenanthrene	-	0.001
Anthracene	-	0.01
Fluoranthene	-	0.001
Pyrene	-	0.001
Benzo[a]anthracene	0.082	0.1
Chrysene	0.017	0.01
Benzo[b]fluoranthene	0.25	0.1
Benzo[k]fluoranthene	0.11	0.1
Benzo[a]pyrene	1.0	1.0
Benzo[g,h,i]perylene	0.19	0.01
Dibenz[a,h]anthracene	0.29	1.0
Indeno[1,2,3-c,d]pyrene	0.31	0.1

- **Results**

Table S8. Element mass fractions (mg kg^{-1} PM_{10}) in road dust samples. The dash indicates elements not detected or below the detection limit.

	min	max
Li	121	412
Be	-	12.5
B	-	-
Sc	8.67	39.4
Ti	3299	12,064
V	61.3	209
Cr	-	762
Mn	565	1921
Co	4.18	30.6
Ni	-	318
Cu	617	4669
Zn	-	3819
Ga	16.0	68.9
Ge	0.965	24.6
As	41.0	165
Se	-	29.3
Rb	190	687
Sr	80.5	493
Y	10.3	43.8
Zr	-	518
Nb	18.8	56.7
Mo	-	1095
Cd	-	23.6
Sn	113	782
Sb	23.7	433
Cs	18.1	59.9
Ba	476	4477
La	24.0	139
Ce	46.9	260
Pr	-	33.6
Nd	22.0	119
Sm	8.04	36.7
Eu	-	2.60
Gd	5.77	33.3
Tb	-	2.21
Dy	2.86	11.1
Ho	-	2.25
Er	-	6.01
Tm	-	-

Yb	-	6.12
Lu	-	-
Hf	-	13.0
Ta	-	2.89
W	-	99.7
Tl	-	4.22
Pb	109	545
Bi	-	45.1
Th	12.1	68.5
U	12.7	37.6
Al	28,880	13,0749
Ca	1075	51,988
Fe	25,965	104,424
K	6446	40,185
Mg	2200	9119
Na	4103	15,719
P	947	3395
S	1317	27,161

Table S9. Correlation matrix between elements (coefficients of correlation, r ≥ 0.7 are in bold).

	Li	Be	Sc	Ti	V	Cr	Mn	Co	Ni	Cu	Zn	Ga	Ge	As	Se	Rb	Sr	Y	Zr	Nb	Mo	Cd	Sn	Sb	Cs	Ba	La	Ce	Pr	Nd	Sm	Gd	Dy	Er	Yb	Hf	W	Pb	Bi	Th	U	Al	Ca	Fe	K	Mg	Na	P	S
Li	1.000																																																	
Be	0.563	1.000																																																
Sc	0.559	-0.174	1.000																																															
Ti	**0.808**	0.181	**0.837**	1.000																																													
V	**0.793**	0.163	**0.807**	**0.989**	1.000																																											
Cr	-0.477	-0.119	-0.276	-0.194	-0.191	1.000																																											
Mn	0.464	0.348	0.218	0.613	0.635	0.501	1.000																																										
Co	-0.378	0.000	-0.539	-0.424	-0.455	**0.715**	0.297	1.000																																									
Ni	-0.559	-0.376	-0.035	-0.361	-0.435	0.556	-0.144	0.600	1.000																																									
Cu	-0.163	0.152	-0.202	0.091	0.128	**0.872**	**0.778**	0.537	0.174	1.000																																								
Zn	0.275	0.190	-0.077	0.407	0.445	0.395	**0.837**	0.331	-0.324	**0.699**	1.000																																							
Ga	**0.843**	0.137	**0.846**	**0.865**	**0.857**	-0.634	0.200	-0.680	-0.473	-0.386	0.035	1.000																																						
Ge	**0.748**	0.293	**0.764**	**0.799**	**0.773**	-0.528	0.222	-0.567	-0.292	-0.242	0.036	**0.886**	1.000																																					
As	**0.869**	**0.761**	0.382	0.628	0.599	-0.553	0.244	-0.523	-0.607	-0.229	0.094	**0.706**	**0.739**	1.000																																					
Se	**0.745**	0.200	**0.801**	**0.885**	**0.894**	-0.493	0.288	-0.775	-0.554	-0.171	0.141	**0.917**	**0.878**	**0.732**	1.000																																					
Rb	**0.974**	0.431	**0.715**	**0.869**	**0.851**	-0.534	0.376	-0.529	-0.527	-0.250	0.158	**0.934**	**0.825**	**0.852**	**0.851**	1.000																																					
Sr	0.554	-0.039	0.562	**0.776**	**0.815**	-0.045	0.568	-0.421	-0.570	0.191	0.521	0.595	0.318	0.345	**0.674**	0.604	1.000																																				
Y	**0.735**	0.149	**0.856**	**0.871**	**0.802**	-0.278	0.378	-0.289	-0.025	-0.130	0.138	**0.829**	**0.873**	0.588	**0.745**	**0.806**	0.411	1.000																																				
Zr	0.202	0.232	0.091	0.392	0.411	**0.737**	**0.942**	0.511	0.144	**0.891**	**0.730**	-0.060	0.004	-0.021	0.026	0.112	0.364	0.212	1.000																																				
Nb	0.566	-0.091	**0.906**	**0.753**	**0.706**	-0.237	0.253	-0.265	0.167	-0.177	-0.055	**0.775**	**0.802**	0.341	0.639	0.671	0.290	**0.919**	0.169	1.000																																				
Mo	-0.255	-0.320	0.022	-0.229	-0.290	-0.013	-0.276	0.413	0.678	-0.209	-0.250	-0.113	0.108	-0.352	-0.320	-0.247	-0.648	0.202	-0.147	0.371	1.000																																				
Cd	-0.604	-0.389	-0.041	-0.442	-0.480	0.504	-0.244	0.452	**0.931**	0.124	-0.499	-0.479	-0.342	-0.639	-0.545	-0.552	-0.579	-0.174	0.070	0.107	0.546	1.000																																			
Sn	-0.180	0.094	-0.222	0.077	0.123	**0.867**	**0.776**	0.549	0.147	**0.995**	**0.734**	-0.395	-0.282	-0.277	-0.192	-0.271	0.220	-0.163	**0.885**	-0.202	-0.211	0.096	1.000																																		
Sb	-0.092	0.155	-0.103	0.175	0.200	**0.872**	**0.823**	0.552	0.229	**0.990**	**0.698**	-0.312	-0.167	-0.191	-0.124	-0.173	0.215	-0.012	**0.934**	-0.057	-0.152	0.157	**0.981**	1.000																															
Cs	**0.973**	0.367	**0.688**	**0.878**	**0.860**	-0.497	0.438	-0.418	-0.509	-0.213	0.277	**0.917**	**0.790**	**0.785**	**0.799**	**0.981**	0.626	**0.821**	0.170	**0.680**	-0.173	-0.580	-0.220	-0.131	1.000																														
Ba	-0.120	0.090	-0.132	0.137	0.167	**0.879**	**0.816**	0.613	0.255	**0.981**	**0.712**	-0.338	-0.214	-0.269	-0.186	-0.210	0.192	-0.043	**0.939**	-0.059	-0.089	0.185	**0.982**	**0.991**	-0.149	1.000																													
La	**0.764**	0.124	**0.845**	**0.904**	**0.892**	-0.441	0.293	-0.723	-0.508	-0.213	0.120	**0.911**	**0.755**	**0.688**	**0.942**	**0.875**	**0.792**	**0.755**	0.041	0.633	-0.409	-0.519	-0.228	-0.152	**0.835**	-0.210	1.000																												
Ce	**0.814**	0.195	**0.836**	**0.940**	**0.940**	-0.439	0.374	-0.699	-0.538	-0.147	0.196	**0.937**	**0.829**	**0.728**	**0.976**	**0.907**	**0.770**	**0.786**	0.113	**0.668**	-0.365	-0.547	-0.163	-0.086	**0.872**	-0.141	**0.984**	1.000																											
Pr	**0.830**	0.333	0.592	**0.887**	**0.933**	-0.289	0.620	-0.516	-0.708	0.123	0.512	**0.800**	**0.683**	**0.690**	**0.867**	**0.844**	**0.830**	0.596	0.353	0.456	-0.500	-0.701	0.127	0.155	**0.842**	0.122	**0.835**	**0.898**	1.000																										
Nd	**0.800**	0.194	**0.868**	**0.925**	**0.910**	-0.459	0.311	-0.711	-0.466	-0.203	0.103	**0.942**	**0.853**	**0.739**	**0.972**	**0.906**	**0.709**	**0.821**	0.062	**0.710**	-0.311	-0.479	-0.228	-0.134	**0.860**	-0.195	**0.984**	**0.992**	**0.842**	1.000																										
Sm	0.461	-0.104	**0.891**	**0.664**	0.610	-0.439	-0.036	-0.539	0.081	-0.381	-0.272	**0.785**	**0.866**	0.420	**0.731**	0.616	0.195	**0.856**	-0.151	**0.906**	0.322	0.041	-0.420	-0.287	0.575	-0.322	**0.678**	**0.693**	0.383	**0.755**	1.000																										
Gd	0.006	-0.565	**0.728**	0.316	0.262	-0.244	-0.279	-0.292	0.438	-0.405	-0.419	0.452	0.496	-0.108	0.339	0.184	-0.028	0.590	-0.261	**0.774**	0.589	0.396	-0.417	-0.322	0.183	-0.312	0.331	0.309	-0.038	0.378	**0.846**	1.000																								
Dy	0.452	0.067	**0.731**	0.543	0.463	0.050	0.266	0.000	0.421	-0.057	-0.209	0.488	0.488	0.263	0.333	0.522	0.150	**0.745**	0.296	**0.822**	0.255	0.389	-0.106	0.073	0.497	0.057	0.444	0.429	0.200	0.497	**0.661**	0.565	1.000																								
Er	0.186	0.488	0.051	0.332	0.334	**0.672**	**0.824**	0.378	0.162	**0.862**	0.544	-0.086	0.143	0.177	0.098	0.108	0.155	0.218	**0.886**	0.134	-0.156	0.114	**0.815**	**0.895**	0.095	**0.852**	0.026	0.114	0.293	0.095	-0.051	-0.276	0.293	1.000																								
Yb	0.186	0.488	0.051	0.332	0.334	**0.672**	**0.824**	0.378	0.162	**0.862**	0.544	-0.086	0.143	0.177	0.098	0.108	0.155	0.218	**0.886**	0.134	-0.156	0.114	**0.815**	**0.895**	0.095	**0.852**	0.026	0.114	0.293	0.095	-0.051	-0.276	0.293	**1.000**	1.000																							
Hf	0.043	-0.488	0.357	0.268	0.277	0.423	0.426	0.378	0.357	0.277	0.250	0.086	-0.143	-0.427	-0.098	0.056	0.367	0.218	0.525	0.401	0.156	0.342	0.321	0.349	0.158	0.427	0.078	0.057	0.098	0.032	0.051	0.276	0.488	0.143	0.143	1.000																						
W	0.521	-0.035	**0.776**	**0.830**	**0.859**	-0.283	0.317	-0.758	-0.501	-0.003	0.212	**0.772**	**0.691**	0.492	**0.933**	**0.656**	**0.788**	0.592	0.101	0.520	-0.438	-0.471	-0.011	0.023	0.608	-0.037	**0.899**	**0.910**	**0.817**	**0.891**	0.619	0.332	0.219	0.118	0.118	0.017	1.000																					
Pb	0.454	-0.026	0.290	0.640	0.645	-0.052	0.542	-0.141	-0.519	0.203	**0.767**	0.428	0.275	0.291	0.487	0.441	**0.780**	0.401	0.308	0.158	-0.336	-0.728	0.246	0.221	0.545	0.214	0.556	0.557	**0.658**	0.490	0.085	-0.082	-0.111	0.088	0.088	0.188	0.550	1.000																			
Bi	0.036	0.183	0.000	0.324	0.357	**0.744**	**0.822**	0.265	-0.061	**0.913**	**0.722**	-0.160	-0.134	-0.019	0.091	-0.014	0.519	0.000	**0.849**	-0.125	-0.517	-0.107	**0.907**	**0.908**	0.000	**0.870**	0.122	0.147	0.365	0.089	-0.286	-0.413	0.000	**0.802**	**0.802**	0.267	0.284	0.427	1.000																			
Th	**0.792**	0.194	**0.874**	**0.879**	**0.863**	-0.553	0.205	-0.750	-0.439	-0.308	-0.012	**0.964**	**0.902**	**0.749**	**0.968**	**0.905**	0.602	**0.827**	-0.039	**0.747**	-0.214	-0.432	-0.336	-0.238	**0.850**	-0.295	**0.953**	**0.969**	**0.792**	**0.987**	**0.818**	0.448	0.511	0.026	0.026	-0.026	**0.854**	0.381	-0.048	1.000																			
U	0.641	0.467	0.104	0.488	0.424	-0.208	0.398	0.000	-0.443	-0.020	0.523	0.371	0.293	0.619	0.333	0.557	0.440	0.447	0.164	0.091	-0.255	-0.701	-0.019	0.021	0.626	-0.013	0.444	0.429	0.467	0.410	0.035	-0.264	0.067	0.098	0.098	-0.098	0.196	**0.735**	0.183	0.335	1.000																		
Al	**0.960**	0.478	0.603	**0.778**	**0.761**	-0.648	0.256	-0.591	-0.643	-0.361	0.113	**0.900**	**0.768**	**0.899**	**0.820**	**0.977**	0.571	**0.705**	-0.036	0.531	-0.321	-0.665	-0.378	-0.302	**0.951**	-0.344	**0.849**	**0.868**	**0.808**	**0.865**	0.528	0.083	0.379	-0.022	-0.022	-0.090	0.611	0.447	-0.101	**0.868**	0.620	1.000															
Ca	-0.317	-0.147	-0.526	-0.234	-0.143	0.573	0.426	0.445	-0.184	**0.649**	**0.654**	-0.509	-0.649	-0.471	-0.405	-0.428	0.267	-0.587	0.487	-0.602	-0.391	-0.166	**0.713**	0.575	-0.340	0.626	-0.366	-0.350	0.017	-0.453	-0.793	-0.650	-0.566	0.234	0.234	0.311	-0.184	0.322	0.611	-0.561	-0.017	-0.424	1.000													
Fe	0.210	0.201	0.148	0.472	0.499	**0.679**	**0.951**	0.398	0.061	**0.902**	**0.799**	0.015	0.123	0.023	0.155	0.140	0.417	0.270	**0.971**	0.206	-0.145	-0.032	**0.897**	**0.938**	0.198	**0.933**	0.118	0.206	0.442	0.149	-0.060	-0.199	0.211	**0.886**	**0.886**	0.427	0.246	0.414	**0.869**	0.050	0.178	-0.007	0.469	1.000											
K	**0.911**	0.348	**0.722**	**0.901**	**0.896**	-0.484	0.397	-0.633	-0.632	-0.183	0.233	**0.915**	**0.760**	**0.819**	**0.911**	**0.960**	**0.769**	**0.736**	0.114	0.569	-0.445	-0.651	-0.196	-0.124	**0.933**	-0.175	**0.955**	**0.965**	**0.908**	**0.952**	0.557	0.129	0.400	0.095	0.095	0.033	**0.798**	0.577	0.128	**0.921**	0.577	**0.951**	-0.302	0.169	1.000									
Mg	**0.862**	0.290	0.602	**0.902**	**0.930**	-0.255	0.650	-0.414	-0.659	0.101	0.547	**0.795**	0.612	**0.655**	**0.802**	**0.864**	**0.880**	0.631	0.387	0.474	-0.484	-0.693	0.112	0.148	**0.889**	0.126	**0.842**	**0.880**	**0.971**	**0.826**	0.345	-0.038	0.277	0.250	0.250	0.238	**0.749**	**0.733**	0.365	**0.759**	0.585	**0.828**	0.049	0.441	**0.922**	1.000							
Na	0.609	0.016	**0.852**	**0.940**	**0.946**	-0.092	0.538	-0.541	-0.334	0.156	0.334	**0.775**	**0.700**	0.486	**0.891**	**0.720**	**0.830**	**0.740**	0.353	**0.660**	-0.360	-0.359	0.143	0.219	**0.697**	0.165	**0.907**	**0.920**	**0.838**	**0.906**	0.642	0.353	0.453	0.320	0.320	0.242	**0.942**	0.595	0.426	**0.848**	0.297	0.626	-0.164	0.458	**0.825**	**0.819**	1.000				
P	**0.796**	0.384	0.458	**0.705**	**0.668**	-0.473	0.271	-0.505	-0.657	-0.248	0.268	**0.706**	0.519	**0.789**	**0.703**	**0.808**	**0.698**	0.567	-0.023	0.278	-0.511	-0.770	-0.255	-0.208	**0.805**	-0.267	**0.821**	**0.782**	**0.717**	**0.772**	0.314	-0.070	0.196	-0.053	-0.053	-0.117	0.594	0.689	0.099	**0.714**	**0.833**	**0.871**	-0.215	0.013	**0.883**	**0.789**	0.611	1.000	-0.519	
S	-0.421	-0.264	-0.420	-0.341	-0.207	0.409	0.172	0.200	-0.130	0.473	0.275	-0.442	-0.547	-0.552	-0.345	-0.471	0.085	-0.670	0.287	-0.490	-0.286	0.075	0.529	0.386	-0.449	0.445	-0.407	-0.362	-0.040	-0.450	-0.616	-0.438	-0.519	0.119	0.119	0.260	-0.130	-0.096	0.362	-0.486	-0.532	-0.492	**0.809**	0.278	-0.386	-0.103	-0.202	-0.519	1.000

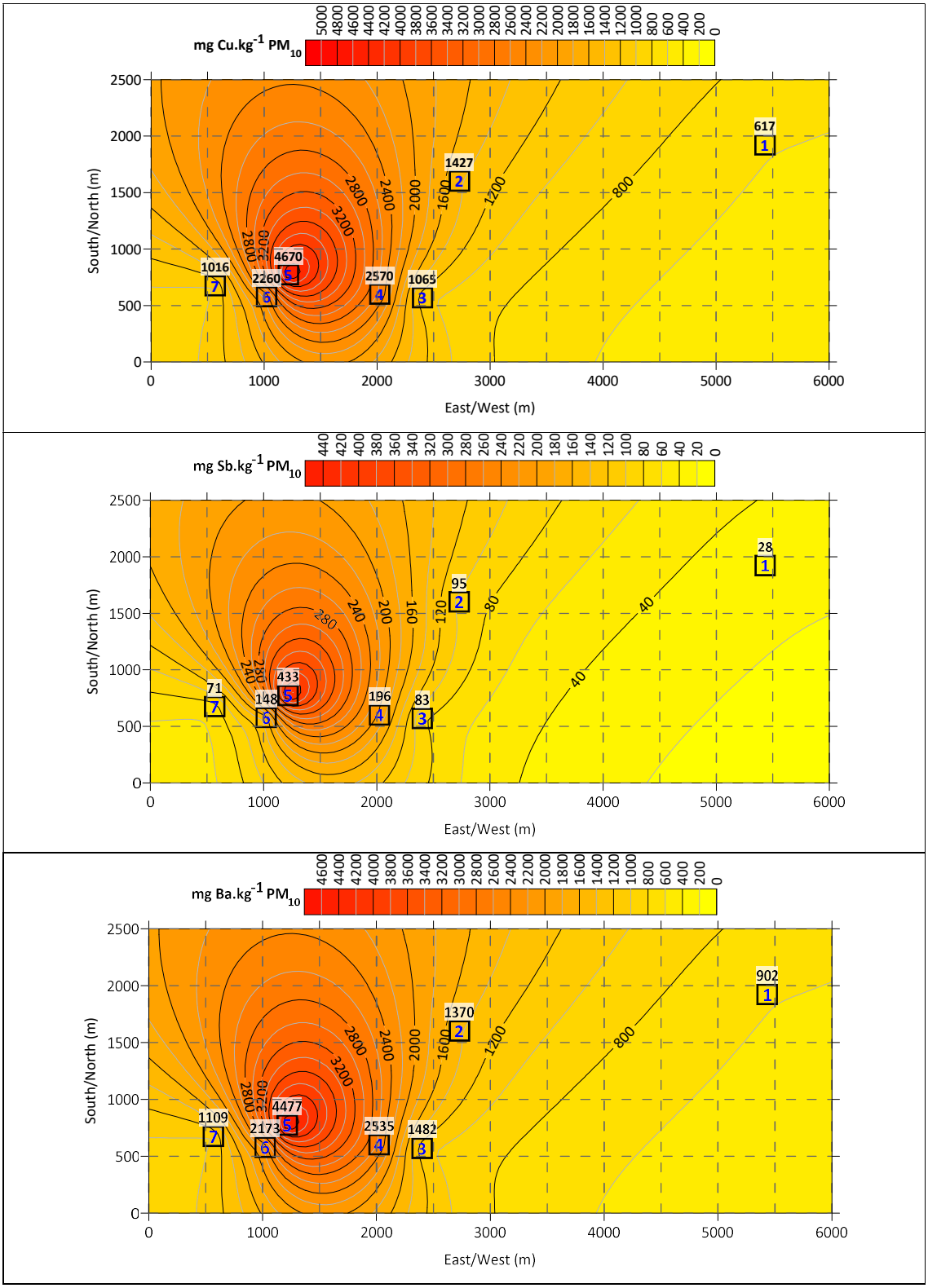
mg Cu.kg-1 PM10
5000 4800 4600 4400 4200 4000 3800 3600 3400 3200 3000 2800 2600 2400 2200 2000 1800 1600 1400 1200 1000 800 600 400 200 0
South/North (m)
East/West (m)
0 1000 2000 3000 4000 5000 6000
0 500 1000 1500 2000 2500
617
1
1427
2
1016
7
4670
5
2260
6
2570
4
1065
3
mg Sb.kg-1 PM10
440 420 400 380 360 340 320 300 280 260 240 220 200 180 160 140 120 100 80 60 40 20 0
28
95
71
433
148
196
83
mg Ba.kg-1 PM10
4600 4400 4200 4000 3800 3600 3400 3200 3000 2800 2600 2400 2200 2000 1800 1600 1400 1200 1000 800 600 400 200 0
902
1370
1109
4477
2173
2535
1482

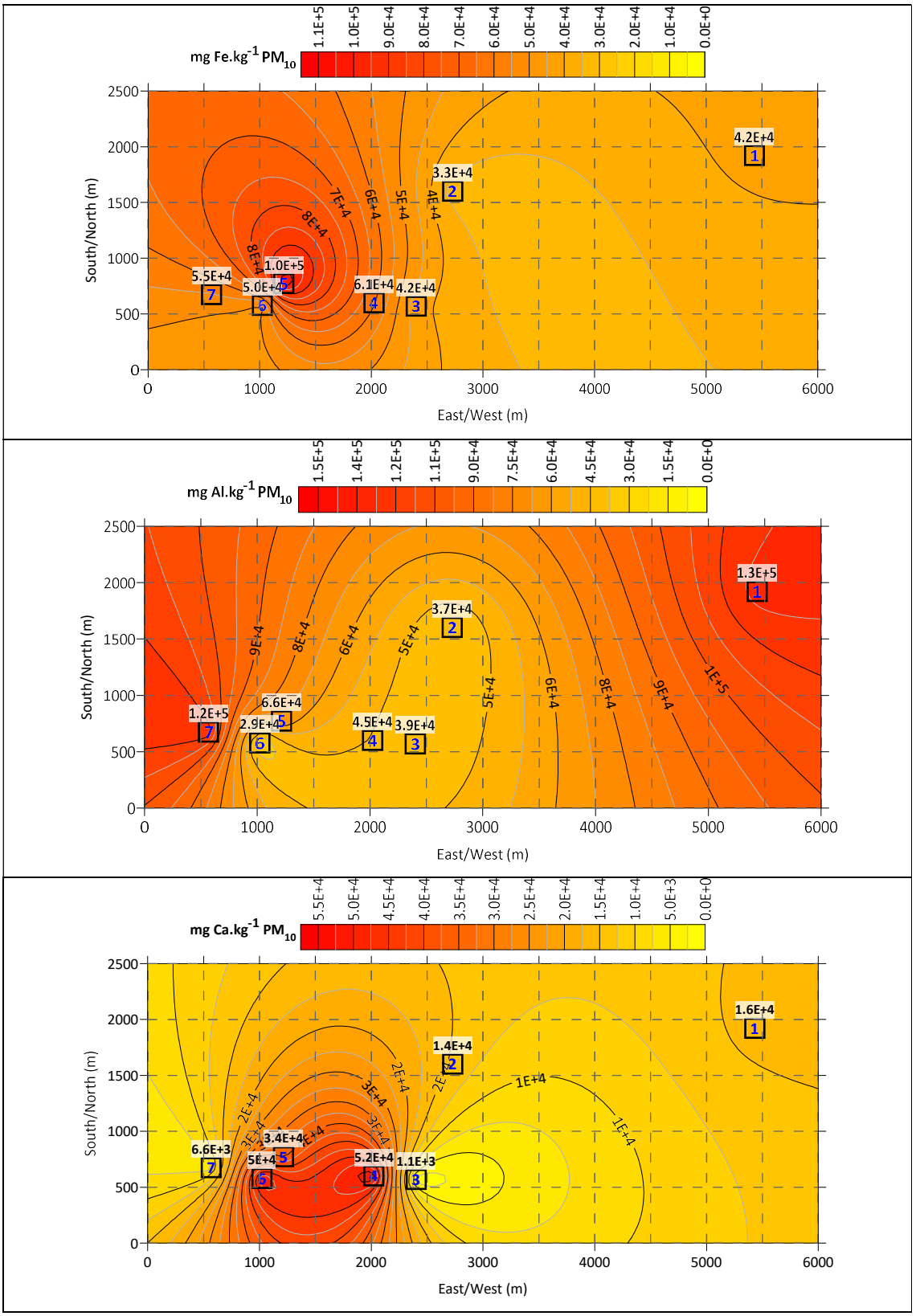
mg Fe.kg-1 PM10
1.1E+5 1.0E+5 9.0E+4 8.0E+4 7.0E+4 6.0E+4 5.0E+4 4.0E+4 3.0E+4 2.0E+4 1.0E+4 0.0E+0
South/North (m)
East/West (m)
4.2E+4
3.3E+4
1.0E+5
5.5E+4
5.0E+4
6.1E+4
4.2E+4
mg Al.kg-1 PM10
1.5E+5 1.4E+5 1.2E+5 1.1E+5 9.0E+4 7.5E+4 6.0E+4 4.5E+4 3.0E+4 1.5E+4 0.0E+0
1.3E+5
3.7E+4
6.6E+4
1.2E+5
2.9E+4
4.5E+4
3.9E+4
mg Ca.kg-1 PM10
5.5E+4 5.0E+4 4.5E+4 4.0E+4 3.5E+4 3.0E+4 2.5E+4 2.0E+4 1.5E+4 1.0E+4 5.0E+3 0.0E+0
1.6E+4
1.4E+4
3.4E+4
6.6E+3
5.2E+4
1.1E+3

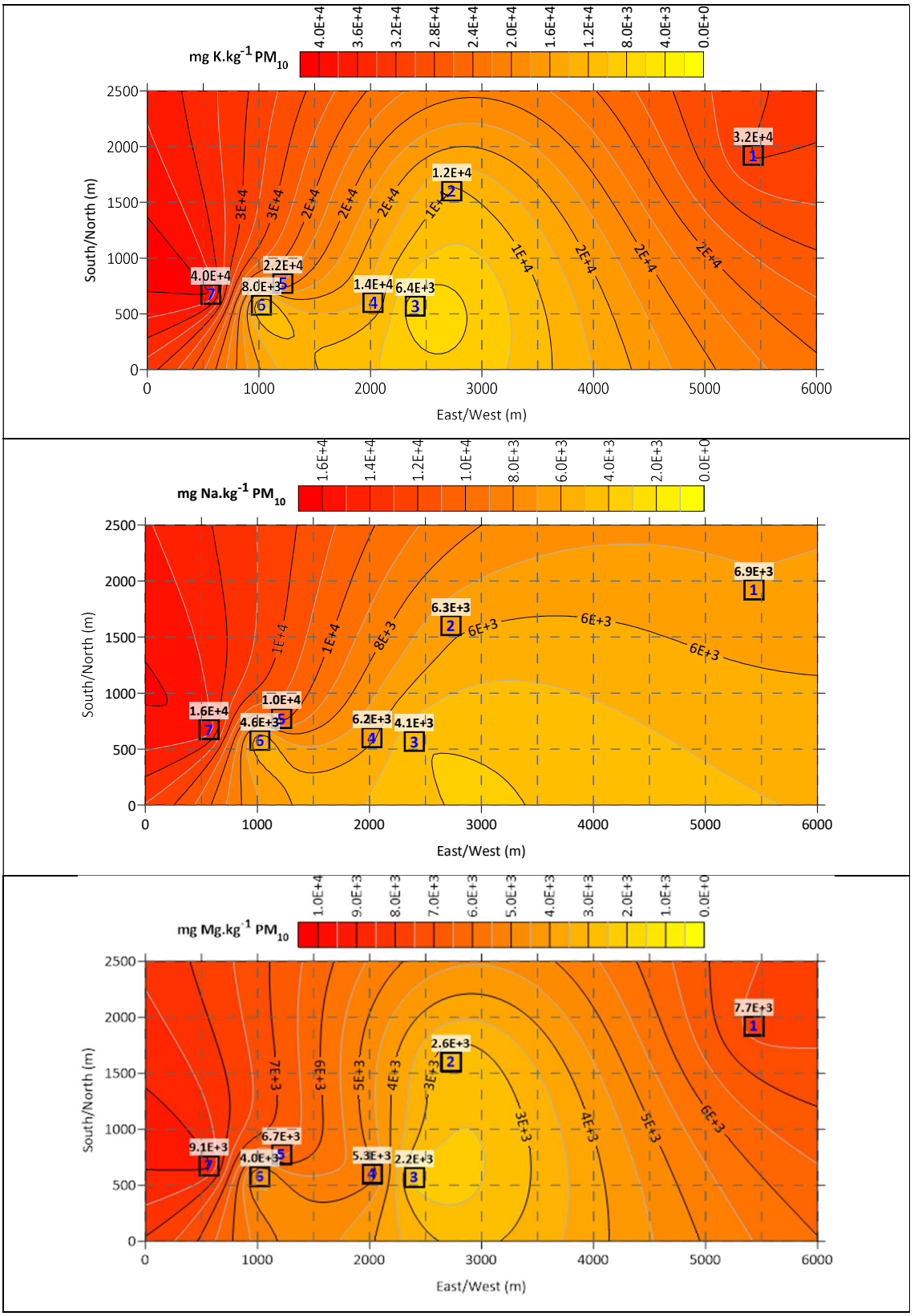
mg K.kg-1 PM10
4.0E+4
3.6E+4
3.2E+4
2.8E+4
2.4E+4
2.0E+4
1.6E+4
1.2E+4
8.0E+3
4.0E+3
0.0E+0
South/North (m)
East/West (m)
3.2E+4
1.2E+4
2.2E+4
4.0E+4
8.0E+3
1.4E+4
6.4E+3
mg Na.kg-1 PM10
1.6E+4
1.4E+4
1.2E+4
1.0E+4
8.0E+3
6.0E+3
4.0E+3
2.0E+3
0.0E+0
6.9E+3
6.3E+3
1.0E+4
1.6E+4
4.6E+3
6.2E+3
4.1E+3
mg Mg.kg-1 PM10
1.0E+4
9.0E+3
8.0E+3
7.0E+3
6.0E+3
5.0E+3
4.0E+3
3.0E+3
2.0E+3
1.0E+3
0.0E+0
7.7E+3
2.6E+3
9.1E+3
6.7E+3
4.0E+3
5.3E+3
2.2E+3

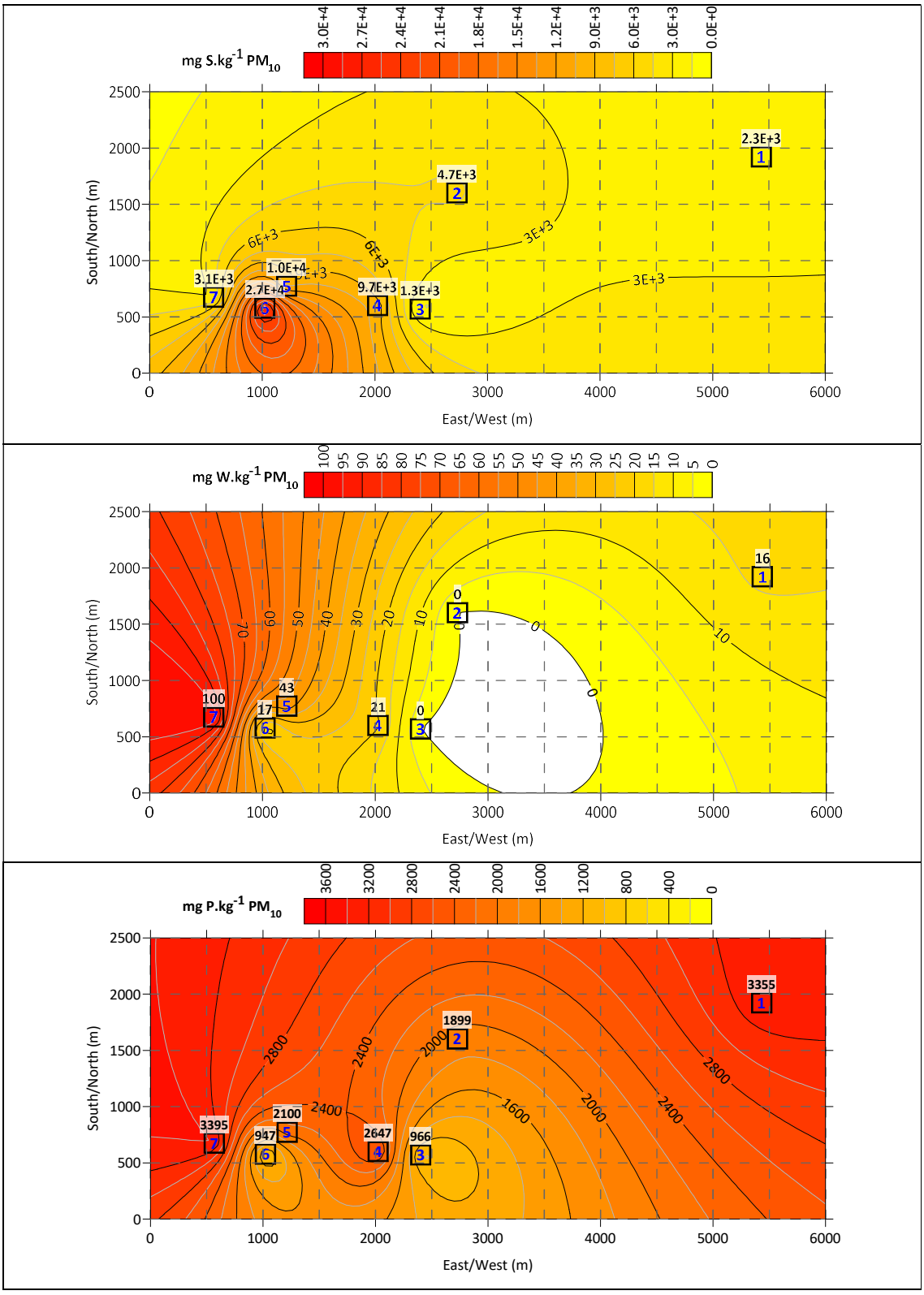
mg S.kg-1 PM10
3.0E+4
2.7E+4
2.4E+4
2.1E+4
1.8E+4
1.5E+4
1.2E+4
9.0E+3
6.0E+3
3.0E+3
0.0E+0
South/North (m)
East/West (m)
2.3E+3
4.7E+3
3.1E+3
2.7E+4
1.0E+4
9.7E+3
1.3E+3
6E+3
3E+3
mg W.kg-1 PM10
100
95
90
85
80
75
70
65
60
55
50
45
40
35
30
25
20
15
10
5
0
16
0
100
43
17
21
0
70
60
50
40
30
20
10
mg P.kg-1 PM10
3600
3200
2800
2400
2000
1600
1200
800
400
0
3355
1899
3395
2100
947
2647
966
2800
2400
2000
1600

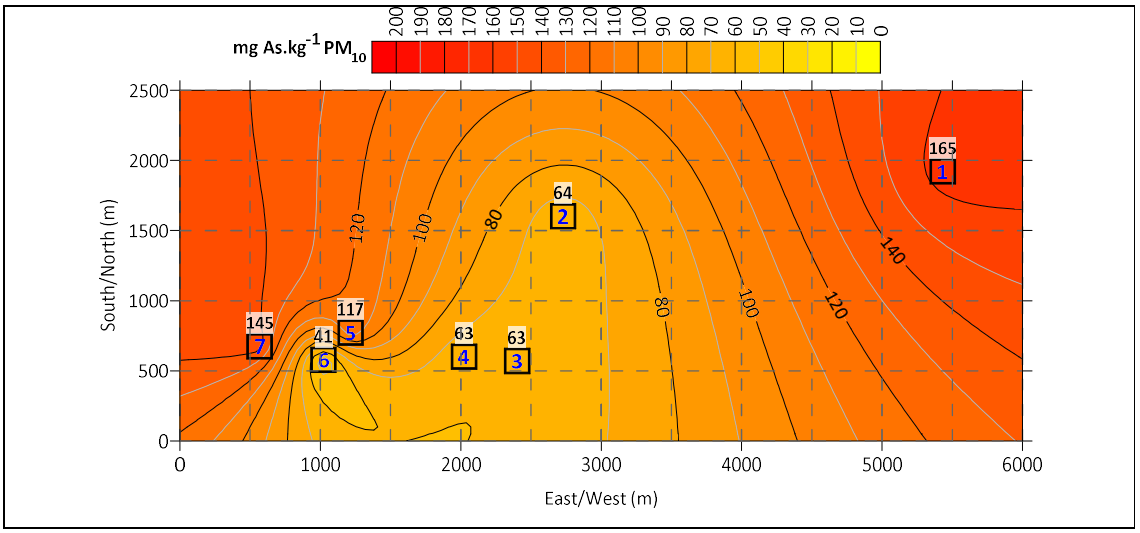

Fig. S2. Spatial distributions of mass concentration for some elements. Squares with blue numbers indicate the streets where sampling was performed:

1 - Rua Alto Xisto - residential area on the outskirts of the city; cobbled pavement made of granite cubes

2 - Av. Capitão Gaspar de Castro - access road to the city centre and residential areas with various public facilities; stone mastic asphalt pavement

3 - Largo João Tomás da Costa - access to the city centre by the river front; stone mastic asphalt pavement

4 - Av. Combatentes da Grande Guerra - central artery connecting to the train station; cobbled pavement made of granite cubes

5 - Av. 25 de Abril - steep exit of a main thoroughfare that crosses the city to a residential neighbourhood; stone mastic asphalt pavement

6 - Av. do Atlântico - avenue of access to the main beach of the city, next to the shipyards; stone mastic asphalt pavement

7 - ESTG - local road within the campus of the Higher School of Technology and Management; stone mastic asphalt pavement

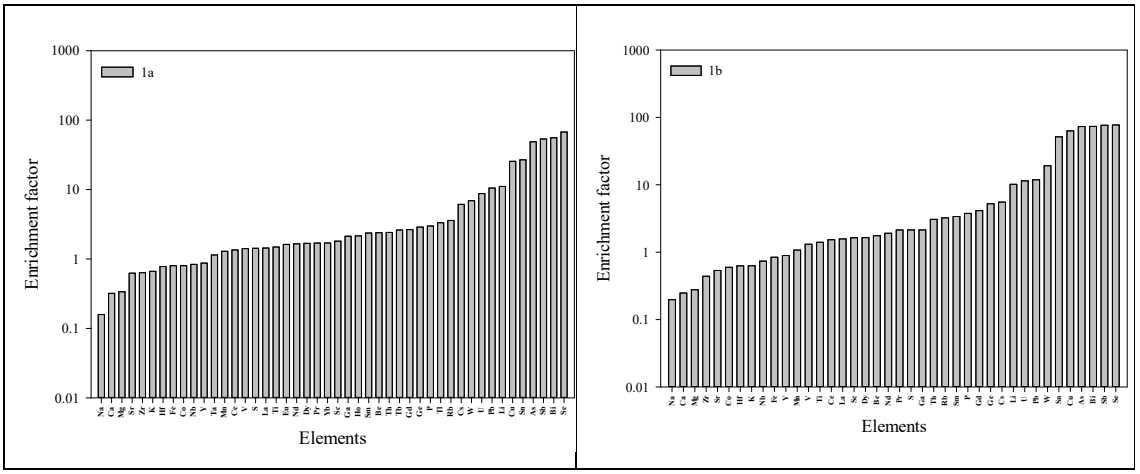

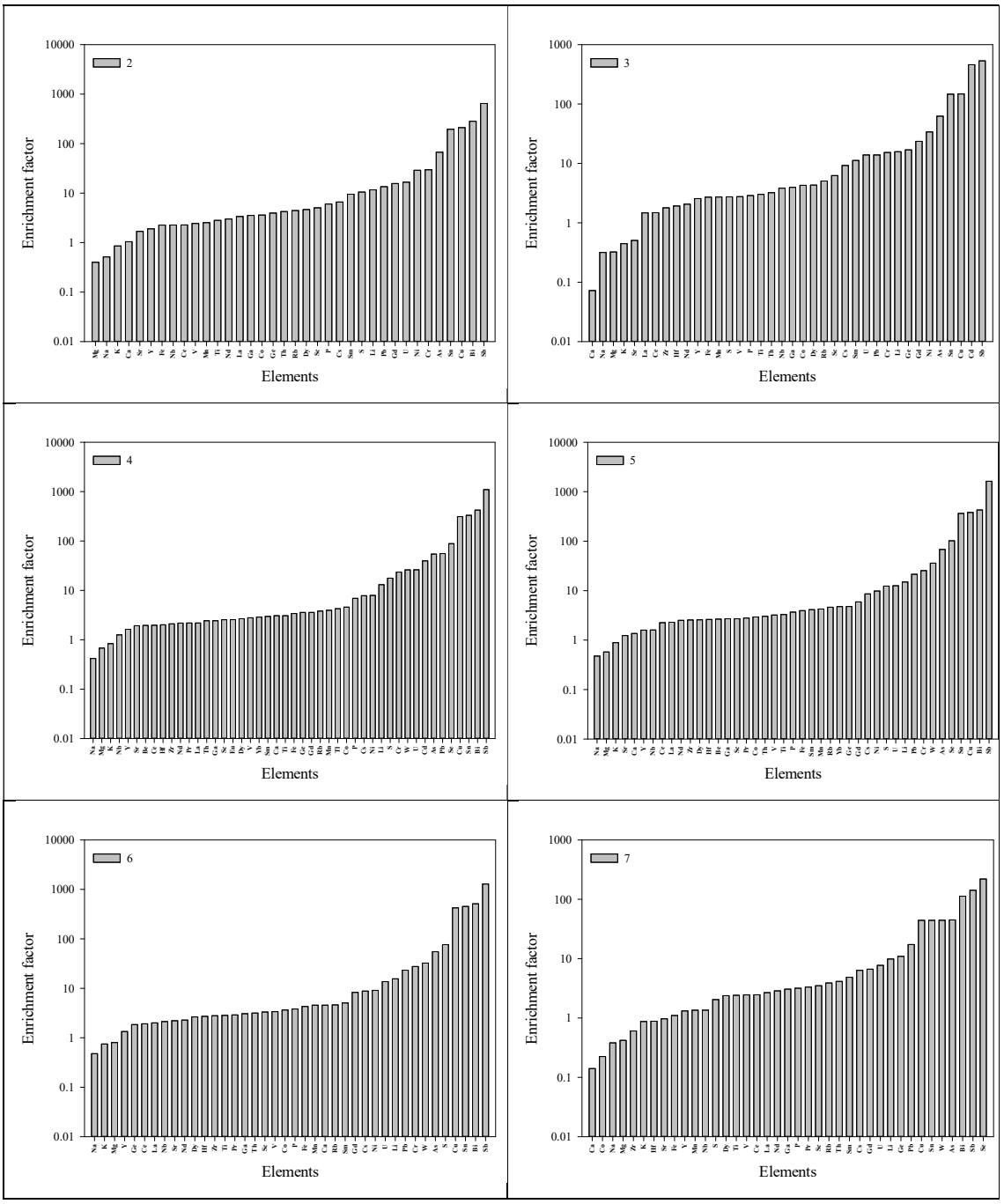

Fig. S3. Enrichment factors for road dust samples. 1a - Rua Alto Xisto, cobbled pavement, before washing; 1b - Rua Alto Xisto, after washing; 2 - Av. Capitão Gaspar de Castro, asphalt pavement; 3 - Largo João Tomás da Costa, asphalt pavement; 4 - Av. Combatentes da Grande Guerra, cobbled pavement; 5 - Av. 25 de Abril - asphalt pavement; 6 - Av. do Atlântico, asphalt pavement; 7 – ESTG, asphalt pavement.

References

Adimalla, N., 2020. Heavy metals contamination in urban surface soils of Medak province, India, and its risk assessment and spatial distribution. Environ. Geochem. Health 42, 59-75.

Błaszczyk, E., Rogula-Kozłowska, W., Klejnowski, K., Fulara, I., Mielżyńska-Švach, D., 2017. Polycyclic aromatic hydrocarbons bound to outdoor and indoor airborne particles ($PM_{2.5}$) and their mutagenicity and carcinogenicity in Silesian kindergartens, Poland. Air Qual. Atmos. Health 10, 389-400.

Faiz, Y., Siddique, N., Tufail, M., 2012. Pollution level and health risk assessment of road dust from an expressway. J. Environ. Sci. Health A Tox. Hazard Subst. Environ. Eng. 47, 818-829.

Ferreira-Baptista, L., de Miguel, E., 2005. Geochemistry and risk assessment of street dust in Luanda, Angola: a tropical urban environment. Atmos. Environ. 39, 4501-4512.

Li, H.-H., Chen, L.-J., Yu, L., Guo, Z.-B., Shan, C.-Q., Lin, J.-Q., Gu ,Y.-G., Yang, Z.-B., Yang, Y.-X., Shao, J.-R., Zhu, X.-M., Cheng, Z., 2017. Pollution characteristics and risk assessment of human exposure to oral bioaccessibility of heavy metals via urban street dusts from different functional areas in Chengdu, China. Sci. Total Environ. 586, 1076-1084.

Xu, X., Lu, X., Han, X., Zhao, N., 2015. Ecological and health risk assessment of metal in resuspended particles of urban street dust from an industrial city in China. Current Sci. 108, 72-79.